

Georgia State University

ScholarWorks @ Georgia State University

Chemistry Theses

Department of Chemistry

12-14-2016

DNA Photo-Cleavage and Interactions by Quinoline Cyanine Dyes; Towards Improving Photodynamic Cancer Therapy

Tayebeh Fatemipouya
tfatemipouya1@student.gsu.edu

Follow this and additional works at: https://scholarworks.gsu.edu/chemistry_theses

Recommended Citation

Fatemipouya, Tayebeh, "DNA Photo-Cleavage and Interactions by Quinoline Cyanine Dyes; Towards Improving Photodynamic Cancer Therapy." Thesis, Georgia State University, 2016.
doi: <https://doi.org/10.57709/9429573>

This Thesis is brought to you for free and open access by the Department of Chemistry at ScholarWorks @ Georgia State University. It has been accepted for inclusion in Chemistry Theses by an authorized administrator of ScholarWorks @ Georgia State University. For more information, please contact scholarworks@gsu.edu.

DNA PHOTO-CLEAVAGE AND INTERACTIONS BY QUINOLINE CYANINE DYES;
TOWARDS IMPROVING PHOTODYNAMIC CANCER THERAPY

by

TAYEBEH FATEMIPOUYA

Under the Direction of Kathryn B. Grant, Ph.D.

ABSTRACT

Photodynamic therapy (PDT) is a cancer treatment method in which a photosensitizer, light of a particular wavelength, and also oxygen are used to destroy cancerous cells. Cancer cells absorb the photosensitizing agent which is injected into the body, and it is triggered to cause cell destruction upon absorption of light. This occurs because of the excitation of the photosensitizer produces reactive oxygen species that induce a cascade of cellular and molecular events in the body. Photosensitizing agents that can photo-cleave DNA at long wavelengths are highly demanded in PDT, because the long wavelengths of light can penetrate through tissue deeply compared to visible light. While most of the photosensitizers are activated at wavelengths less than 690 nm, penetration of light continues to increase at increasing wavelengths. In this thesis, photosensitizers that can be activated to oxidize DNA with long wavelengths of light will be discussed. Using quinoline cyanine dyes, here we report the first example of DNA photocleavage at a wavelength of light above 800 nm.

INDEX WORDS: Cyanine dye, DNA, Cancer treatment, Gel electrophoresis, UV-visible
spectroscopy

DNA PHOTO-CLEAVAGE AND INTERACTIONS BY QUINOLINE CYANINE DYES;
TOWARDS IMPROVING PHOTODYNAMIC CANCER THERAPY

by

TAYEBEH FATEMIPOUYA

A Thesis Submitted in Partial Fulfillment of the Requirements for the Degree of

Master of Science

in the College of Arts and Sciences

Georgia State University

2016

Copyright by
TAYEBEH FATEMIPOUYA
2016

DNA PHOTO-CLEAVAGE AND INTERACTIONS BY QUINOLINE CYANINE DYES;
TOWARDS IMPROVING PHOTODYNAMIC CANCER THERAPY

by

TAYEBEH FATEMIPOUYA

Committee Chair: Kathryn B. Grant

Committee: Maged Henary

W. David Wilson

Electronic Version Approved:

Office of Graduate Studies

College of Arts and Sciences

Georgia State University

December 2016

TO MY PARENTS, MY LOVELY SISTERS AND BROTHER
AND MY LOVE, ALIREZA

ACKNOWLEDGEMENTS

I would like to acknowledge my advisor, Dr. Kathryn Grant for taking me in as a graduate student and molding me into the scientist I have become. She always motivated me and was optimistic even when my experimental results were unexpected. I thank her for all her support and teaching me to always reach for the best.

To my lab mates, both past and present, it was a pleasure to work with you all. I will never forget our wonderful time in the lab. I count myself lucky to call you colleagues.

Last but not least, I would like to thank my committee members, Dr. Henary and Dr. Wilson for accepting the position despite their busy schedules. Thank you both for looking out for my best interests.

TABLE OF CONTENTS

ACKNOWLEDGEMENTS	v
LIST OF TABLES	ix
LIST OF FIGURES	x
1 INTRODUCTION	1
1.1 Polymethine cyanine dyes and structural features.....	1
<i>1.1.1 Cyanine dye interactions with DNA</i>	<i>2</i>
<i>1.1.2 Cyanine dye aggregation</i>	<i>3</i>
<i>1.1.3 DNA binding modes</i>	<i>4</i>
<i>1.1.4 Photodynamic therapy</i>	<i>4</i>
<i>1.1.5 Photosensitizers</i>	<i>6</i>
<i>1.1.6 Infrared photosensitizing agents</i>	<i>10</i>
1.2 Summary of the research.....	12
2 EXPERIMENT	14
2.1 Materials	14
2.2 Instruments	15
2.3 Method.....	16
<i>2.3.1 UV-visible absorption.....</i>	<i>16</i>
<i>2.3.2 Preparation of agarose gel.....</i>	<i>16</i>
<i>2.3.3 Preparation of sodium phosphate buffer and samples</i>	<i>16</i>

2.3.4	<i>Plasmid DNA photocleavage</i>	17
2.3.5	<i>DNA photocleavage time course experiments</i>	18
2.3.6	<i>Fluorescence spectroscopy</i>	18
2.3.7	<i>Circular dichroism</i>	20
2.3.8	<i>Binding constant</i>	20
2.3.9	<i>Anaerobic photocleavage of plasmid DNA</i>	21
2.3.10	<i>Singlet oxygen and hydroxyl radical generators</i>	22
3	RESULTS AND DISCUSSION	23
3.1	UV-Visible absorption analysis of cyanine dyes	23
3.1.1	<i>Time course UV-visible absorption study for dyes</i>	23
3.2	PUC19 plasmid DNA cleavage analysis	27
3.2.1	<i>Photocleavage of supercoiled plasmid DNA at 808 nm, 830 nm, 850 nm..</i>	27
3.2.2	<i>Temperature-dependent experiments</i>	30
3.2.3	<i>Time course photocleavage</i>	33
3.2.4	<i>Concentration titration of cyanine dyes 1 and 2</i>	35
3.2.5	<i>Photocleavage mechanism of dyes 1 and 2</i>	37
3.2.6	<i>Photocleavage of pUC19 DNA, scavenger assay</i>	38
3.2.7	<i>Hydrogen peroxide measurement using Amplex Red</i>	39
3.2.8	<i>Hydrogen peroxide scavenger, catalase</i>	41
3.2.9	<i>Deuterium oxide, singlet oxygen potentiator</i>	42

3.2.10	<i>Anaerobic photocleavage of plasmid DNA using a glove box</i>	44
3.2.11	<i>CT DNA absorption titration and induced circular dichroism data</i>	46
3.2.12	<i>Determination of the dye binding constants (K_b)</i>	50
4	CONCLUSIONS	53
	REFERENCES	55
	APPENDICES	63
	Appendix A	63
	<i>Appendix A.1</i>	63

LIST OF TABLES

Table 1. Time course analysis reaction conditions	18
Table 2. Average inhibition % of DNA photo cleavage induced by ROS scavengers, D ₂ O, catalase and anaerobic condition in glove box.....	46

LIST OF FIGURES

Figure 1.1 Generic structure of cyanine dye and common heterocyclic component. R refers to substituents, mainly alkyl groups.	2
Figure 1.2 Examples of symmetrical (left) and unsymmetrical (right) cyanine dyes.....	2
Figure 1.3 Graphical illustration of the photophysical and photochemical mechanisms of a photosensitizer.....	6
Figure 1.4 Schematic representation of photodynamic therapy. [4].....	7
Figure 1.5 Chemical structure of FDA approved photosensitizers. [29], [30]	10
Figure 1.6 Chemical structures of photosensitizers that absorb long wavelengths of light	12
Figure 1.7 Synthesized cyanine dyes by Dr. Henary's lab at Georgia State University...	14
Figure 2.1 Conversion of Amplex Red into Resorufin.....	19
Figure 3.1 Time course UV-visible absorption spectra of cyanine 1 , 2 and 3 in DMSO.	24
Figure 3.2 Absorption spectra upon adding calf thymus DNA.	25
Figure 3.3 Time course UV-visible absorption study in the absence of CT-DNA.....	26
Figure 3.4 Time course UV-visible absorption study in the presence of CT-DNA.	27
Figure 3.5 Agarose gel electrophoresis of supercoiled pUC19 plasmid DNA with an 808 nm laser.	29
Figure 3.6 Agarose gel electrophoresis of supercoiled pUC19 plasmid DNA.....	30
Figure 3.7 Dark control reactions.	31
Figure 3.8 Temperature dependent experiment at 830 nm, 300 mW.	32
Figure 3.9 Temperature dependent experiment at 850 nm 100 mW.	32
Figure 3.10 Temperature dependent experiment at 808 nm.	33

Figure 3.11 Time course experiment for dye 1	34
Figure 3.12 Time course experiment for dye 2	34
Figure 3.13 Concentration titration experiment for dye 1	36
Figure 3.14 Concentration titration experiment for dye 2	37
Figure 3.15 Mechanisms of action in photodynamic therapy.....	38
Figure 3.16 Photocleavage with scavengers sodium benzoate and sodium azide.	39
Figure 3.17 Hydrogen peroxide measurement using Amplex Red.....	41
Figure 3.18 Photographs of 1.5% nondenaturing agarose gel with catalase.	42
Figure 3.19 DNA photocleavage by Compound 1 in the presence and absence of D ₂ O 70% (v/v).	43
Figure 3.20 DNA photocleavage by Compound 2 in the presence and absence of D ₂ O 70% (v/v).	44
Figure 3.21 Aerobic and anaerobic cleavage experiments using glove box.....	45
Figure 3.22. CT DNA concentration titration of dye 1 and dye 2	47
Figure 3.23. Circular dichroism (CD) spectra of A) dye 1 and B) dye 2 in the presence and absence of DNA.	50
Figure 3.24 Representative plots for the interaction of 120 μ M of CT-DNA and 10 μ M of dye 1 and 2 and 10 mM of sodium phosphate buffer, pH 7.0. Linear fitting to Meehan and coworker's binding model generated the curves shown above. The plots were prepared using absorbance at the λ_{\max} value of the dyes 1 and 2	52
Figure 0.1 CT-DNA concentration titration of dyes 1 and 2 from 200 nm to 900 nm.....	63
Figure 0.2 control experiment for H ₂ O ₂ detection using Amplex Red.	64
Figure 0.3 CT-DNA concentration titration of dye 1 and 2 from 400 nm to 900 nm.....	65

1 INTRODUCTION

1.1 Polymethine cyanine dyes and structural features

Cyanine dyes are among the oldest classes of synthetic compounds and continue to find applications in a variety of fields. The generic cyanine dyes consist of two aromatic heterocyclic nitrogen rings, one of which is positively charged and is linked by a conjugated chain of an odd number of carbon atoms to the other nitrogen. [1] The spectra of cyanine dyes depend on the length of this polymethine bridge. In many cases, the dyes act as fluorescence probes for biomolecules, and can interact with the biomolecule either through covalent or noncovalent bonding. [1] Common heterocycles include indole, quinoline, benzoxazole, and benzothiazole rings. [1]

The cyanine dyes conjugated system is varied in increments of two carbons, based on the length of the polymethine bridge separating the two nitrogen atoms. Because this bridge has an odd number of carbons, the positive charge is delocalized by resonance over both nitrogen rings. [1]

Cyanine dyes are planar cationic molecules. The structures of typical dyes are shown in Figures 1.1 and 1.2. The number of carbon atoms in the chain and the nature of the ring containing the nitrogen atoms can vary. The R groups in the diagram represent H, CH₃, CH₃CH₂, or many other groups. These dyes are cations so that they can be paired with many anions, *e.g.* I⁻, Br⁻, Cl⁻, and others. The wavelength and absorption band depends on the length of the methine chain between the nitrogen rings and the nature of the heterocyclic rings.

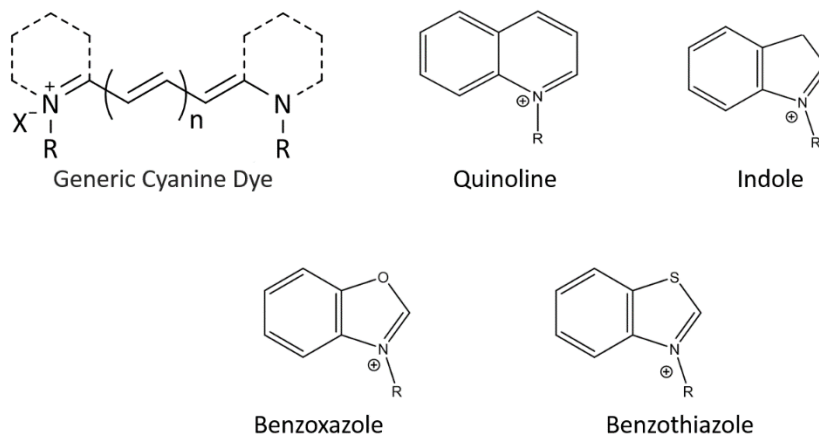


Figure 1.1 Generic structure of cyanine dye and common heterocyclic component. R refers to substituents, mainly alkyl groups.

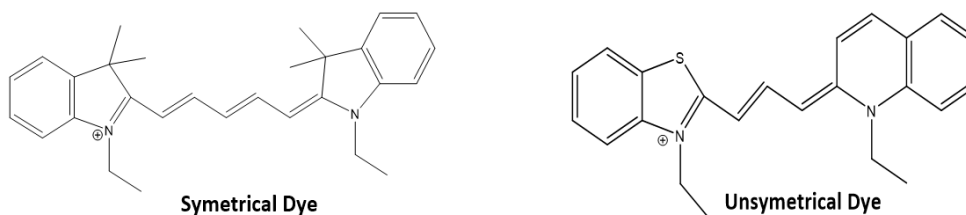


Figure 1.2 Examples of symmetrical (left) and unsymmetrical (right) cyanine dyes.

1.1.1 Cyanine dye interactions with DNA

Studying interactions of cyanine dyes with DNA has been related mainly to applications in the life sciences and biotechnology. However, recent work has shown that cyanine dyes can also assemble into interesting supramolecular aggregates by using DNA as a template. These findings, which are consistent with the well-known propensity of cyanines to aggregate in aqueous solution and on a variety of synthetic and biological surfaces, are taking cyanine dye research into the area of materials science and nanotechnology. [2] cyanine dyes that bind to the minor grooves of DNA shows high selectivity for DNA sequences, suggesting detection of specific base pairs. Cations have electrostatic interactions with DNA because of its poly-anionic nature. Thus, influences and the interactions among dyes can either enhance or suppress aggregation. [3] The interactions between dyes and DNA are very sensitive to other factors.

Besides molecular size, environmental conditions such as dye concentrations and pH have an important effect on dye interactions with DNA. [3] Dyes with a short polymethine bridge can intercalate into DNA even when the concentration of DNA is low. In this case, cyanine dye fluorescence increases by increasing the concentration of DNA until the dye is saturated and the spectral shape that we observe does not change. When the polymethine bridge is longer, monomeric molecules form complex aggregates with small amounts of DNA accompanied by fluorescence quenching. However, when we increase the amount of DNA, the fluorescence efficiencies are enhanced, an indication that dye molecules and DNA strand form a polyionic complex. [3]

1.1.2 Cyanine dye aggregation

Cyanine dyes are known for self-aggregation in polar solutions. This feature of cyanine dyes plays a major role in fluorescent probe development. Depending on the angle of slippage, there are two types of cyanine aggregation, namely H and J-aggregates. [1] Red shifted J-aggregation is the most commercially important dye assemblage for photographic spectral sensitization. [4] The type of aggregation for a dye depends on a number of factors, such as the dye concentration and structure, pH, ionic strength and polarity of the solvent. A molecule that aggregates in a parallel way forms H-dimers or in a head-to-tail arrangement forms J-dimers. [4] Armitage pointed out that unsubstituted dyes are more likely tend to undergo H-aggregation to minimize exposure to water molecules. On the other hand, substituted dyes participate in J-aggregation. [1] For dyes with a long polymethine bridge “degradation” is another concern. Light and molecular oxygen are two factors that have important effects on dye decomposition. Cyanine dyes are bleached by singlet oxygen ($^1\text{O}_2$) or by superoxide anions ($\text{O}_2^{\cdot-}$) in redox reactions.

1.1.3 DNA binding modes

Based on the structural features of cyanine dyes, many can bind to DNA. Depending on the dye's structure, there are three major binding modes: groove, intercalative and external binding. Positively charged ligands are attracted to the negatively charged phosphodiester groups of the DNA. Large molecules like proteins can bind to the double helix within major groove, while it is rare for small molecules. Cationic molecules which have planar aromatic rings interact with DNA via intercalation. On the other hand, minor groove binding needs ligands with structural flexibility. The minor groove binding molecules must adjust their structures by twisting in order to insert into the curve of the minor groove of the double helix. That is why compared to intercalators, groove binder causes less distortion to DNA structure. [1] Among the factors governing the binding modes, it appears that the most significant is molecular shape. Those complexes that fit best with the DNA helical structure display the highest binding affinity. [5] Cyanine dye DNA binding modes can vary according to the nature of the heterocyclic nitrogen ring and its substituents as well as the polymethine chain. Also, nature and charge of the substituents has an effect on the DNA binding mode. [6] Many carbocyanine dyes bind to DNA due to intercalation or groove binding depending on the dye structure. [1], [3], [7] The identity of the terminal heterocyclic group and the length of the polymethine chain have a substantial effect on the photo-physical properties of carbocyanine dyes as well. [1]

1.1.4 Photodynamic therapy

Photodynamic therapy (PDT) is a cancer treatment method in which there are dyes known as photosensitizers (PS) that either are systemically, locally or topically administered to a patient bearing a lesion, followed by exposure to visible light. In the presence of oxygen, this leads to the generation of singlet oxygen and other cytotoxic reactive oxygen species (ROS) that

consequently cause cell damage and tissue destruction. [8] Typical photosensitizers are clinically used in dermatology or skin treatment because light can be applied directly to the skin, offering minimum phototoxicity to healthy cells, a known side effect of systemic photosensitizers. [9] Because the photosensitizer and light can be efficiently delivered to the skin directly, PDT is used increasingly as a therapy in dermatology, in the treatment of skin tumors and, infectious skin disorders. [9] For getting the best results in PDT, several properties of a photosensitizer are needed. First, the PS should be pure and should have a high quantum yield of reactive oxygen species. Secondly, it should have minimum dark toxicity and have maximum solubility in aqueous solutions. One of the most important properties of a PS is long wavelength absorption for efficient medical treatment. [10]

Commonly, the optical absorption of proteins is measured between 275 nm to 280 nm. [11] The wavelength of maximum absorption for both DNA and RNA is 260 nm ($\lambda_{max} = 260$ nm) with a characteristic value for each base. The maximum absorption peaks at 540 nm and 575 nm are for oxy-hemoglobin, and at 555 nm for deoxy-hemoglobin. Because of the background light absorption by water, hemoglobin, DNA, protein and other chromophores in the body, the ideal photosensitizer agent will absorb the light from 700 nm to 1200 nm when there is maximum light penetration in the tissues. Penetration of light through tissues is determined by two mechanisms: light scattering and light absorption. [12], [11]. Typically, red light (630 nm) can penetrate to a depth of 2–3 mm, whereas longer wavelengths (700–800 nm) can penetrate further, up to 5–6 mm. [13], [11] Therefore, near infrared (NIR) polymethine cyanine dyes that have excellent photophysical properties are ideal to be explored as PDT drugs for clinical use. [14], [15] As it shown in Figure 1.3, in the PDT process, there are two typical pathways in which photosensitizers generate reactive oxygen species (ROS). In type one reactions,

photosensitizers in the triplet state, react with the substances such as the cell membrane directly and transfer electrons to oxygen to generate the superoxide anion radical ($O_2^{\cdot-}$) which leads to the production of H_2O_2 and highly reactive hydroxyl radicals ($\cdot OH$). In the second type of reactions, the triplet state of the photosensitizer transfers its energy to the ground triplet state oxygen (3O_2), converting it to excited state singlet oxygen (1O_2). The ratio between these processes depends on the type of the PS and the concentrations of PS and oxygen.

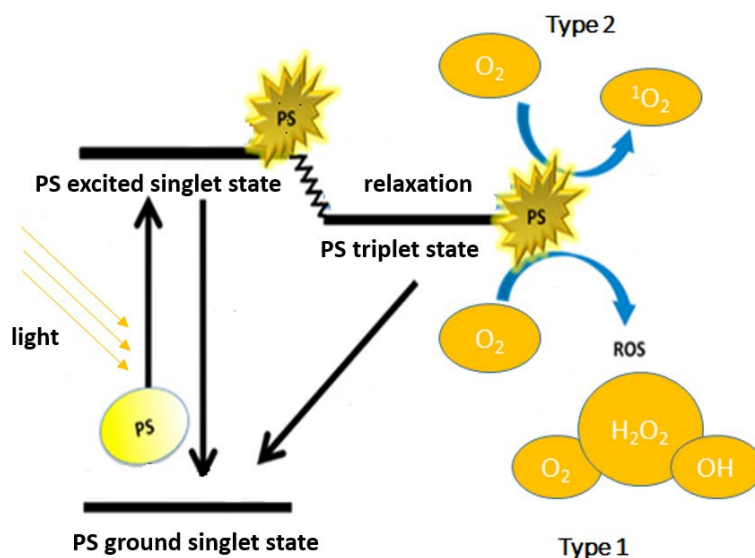


Figure 1.3 Graphical illustration of the photophysical and photochemical mechanisms of a photosensitizer

1.1.5 Photosensitizers

A photosensitizer (PS) is a molecule triggered by light to cause a photochemical reaction with a target molecule. When the PS is exposed to the appropriate wavelength of light, it is activated from the ground state, S₀, to the excited state, S₁. The PS then undergoes intersystem crossing to a long-lived excited triplet state, T₁, from which the ROS, singlet oxygen (¹O₂), and superoxide anion radicals ($O_2^{\cdot-}$) are generated. Figure 1.4 shows four steps of photodynamic therapy.

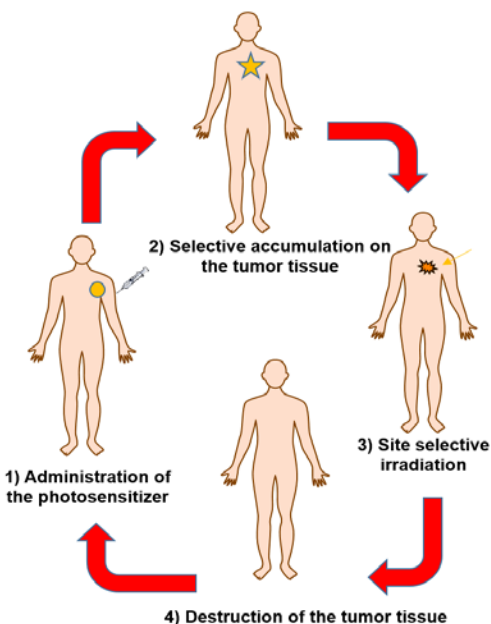


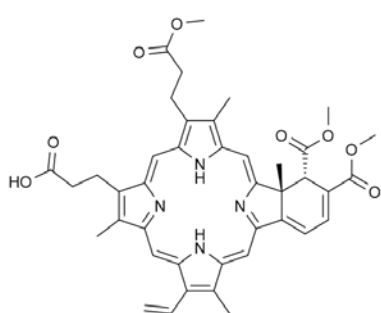
Figure 1.4 Schematic representation of photodynamic therapy. [4]

As mentioned, absorption of UV light and visible light by molecules of our body suggest that there is an “optical window” of 700 nm to 1200 nm for maximum transmittance of light. [16], [17] Interestingly, most photosensitizing agents in clinical use are activated outside of the range of the optical window (700 nm to 1200 nm). There are a number of FDA-approved photosensitizers (Figure 1.5), one of the most commonly used PS is Porfimer (Photofrin[®]), which is activated with 630 nm red light. [17]. Photofrin is a highly selective photosensitizer because it accumulates in the tumor tissue, and thus the Photofrin concentration in the tumor tissue is substantially higher than in the healthy tissues. [18], [19] Verteporfin (Visudyne[®]) is an effective FDA approved photosensitizer for the treatment of age-related macular degeneration (ARMD), which is the leading cause of irreversible blindness in people 50 years of age or older in the developed world. It is also used to treat pathologic myopia. [20] Verteporfin is activated by light sources that emit at 417 nm and 635 nm. Photodynamic therapy with the use of Verteporfin as a photosensitizer is also useful in treating vascularized tumors, and

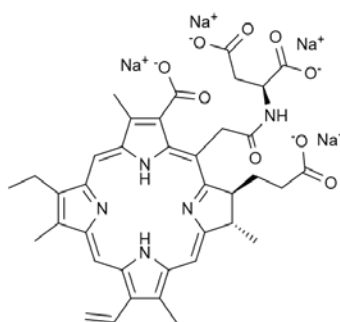
neovascularization which is the development of new blood vessels, especially in tissues where diseases have impaired circulation. [11] Temoporfin (Foscan[®]) is a second generation photosensitizer. It has shorter periods of photosensitivity, longer activation wavelengths, and therefore increased tissue depth of effectiveness. Thus this PS is activated at 652 nm and has a residual photosensitivity of only two weeks. [21] It is used to treat patients with head and neck cancer. [22] Talaporfin sodium is a water-soluble chlorine derivative that has a peak absorption at approximately 400 nm, with the strongest Q-band at 664 nm in plasma. It has been shown to have a high affinity for albumin and other plasma proteins. [23] This photosensitizer is used to treat advanced age-related macular degeneration and patients with refractory colorectal liver metastases. Photolon[™] has two absorption peaks at approximately 420 and 660 nm. [24] This long wavelength of the activation means that Photolon[™] can be used for deep tissue excitation, and thus the destruction of deep-seated tumors. Photolon[™] has been used successfully in the treatment of head, neck, and skin melanomas, where the early stage cancerous growths disappeared in 95% of cases. [25]

Figure 1.5 shows the structure of the FDA approved photosensitizing agents. Indocyanine green (ICG) is a sterile, anionic, water-soluble but relatively hydrophobic, tri carbocyanine molecule. It is a negatively charged ion that belongs to the large family of cyanine dyes. Dry ICG is stable at room temperature. The ICG dye was approved for clinical use in 1959 by FDA for fluorescence imaging. [26], [27] Fluorescence imaging using ICG has become widespread as an intraoperative navigation tool to study lymphatic flow in the extremities and image lymph nodes in patients with breast cancer. Following intravenous injection, ICG is rapidly bound by plasma proteins. ICG becomes fluorescent once excited using near infra-red (NIR) light at about 820 nm and longer wavelengths. The absorption peaks of ICG is around

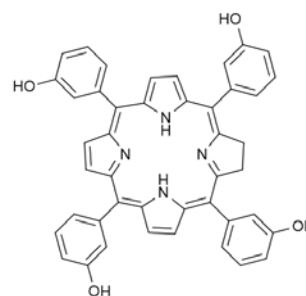
807 nm, and the emission peak is around 822 nm. [27], [26] The fluorescence released by ICG can be detected using specially designated scopes and cameras. Excited ICG is proposed to produce singlet oxygen, which is a strongly cytotoxic agent. Engel et al. have recently studied the stability of ICG when exposed to light and the consequences of singlet oxygen production by ICG. [28] According to their observations, the decomposition of ICG is due to singlet oxygen, but it seems that the singlet oxygen is immediately bound to the decomposition products of ICG itself.



Verteporfin (Visudyne®)



Talaporfin (Laserphyrin®)



Temoporfin (Foscan®)

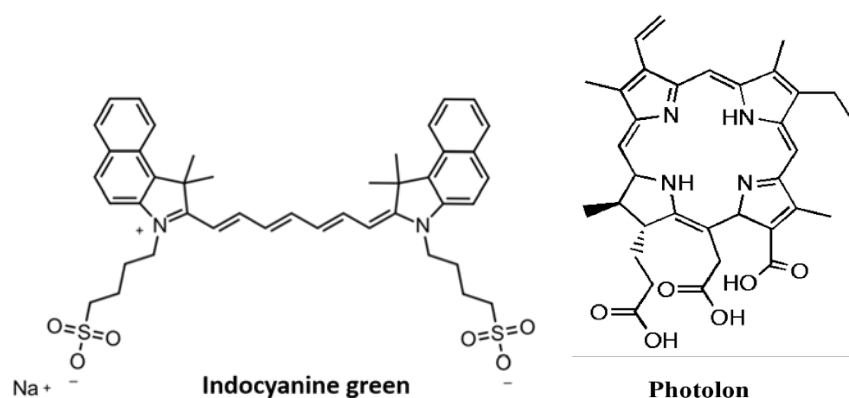
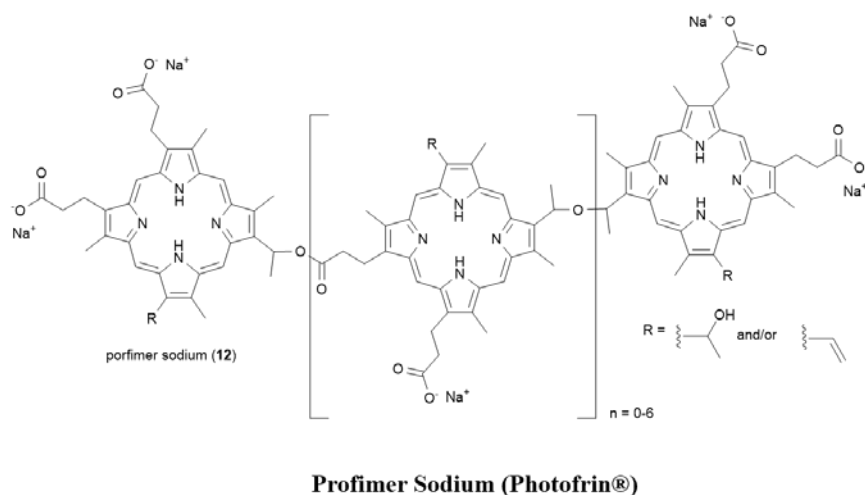


Figure 1.5 Chemical structure of FDA approved photosensitizers. [29], [30]

1.1.6 Infrared photosensitizing agents

As previously stated, the ideal photosensitizer for photodynamic therapy (PDT) should meet many requirements *e.g.*, chemical purity, minimal dark toxicity, significant light absorption at wavelengths that penetrate tissue deeply, high tumor selectivity and rapid clearance from normal tissue. [31] Photosensitizers that are excitable with infrared light have greater tissue penetration depth than most existing photosensitizers that absorb light in the visible range. [32], [33] In order to increase the tissue penetration depth, most of the second-generation photosensitizers (PS) used for cancer therapy are therefore designed to efficiently absorb the light in the longer wavelength region above 700 nm, where the light has a deeper penetration

depth in bio-tissues. [34] Excitable photosensitizers at short wavelengths of light (UV and blue light) are usually ignored for cancer therapy, because of their extremely low tissue penetration depth (less than 1 mm), resulting in ineffective therapeutic effects in the case where the cancer cells are not located near the superficial skin surface. [34], [35], [36] Compared with UV-visible light, near-infrared (NIR) irradiation shows lower photodamage effects and a higher signal-to-noise ratio in fluorescence imaging. [37]

As we discussed previously, in biomedical applications, we require a considerably deeper penetration of near-infrared (NIR) light. In the NIR region, because of weak scattering and energy absorption we have optimal tissue transmission, thus it provides maximum irradiation penetration through the tissue and minimizes the autofluorescence of the non-target tissue. [33] These features make it more ideal for effective phototherapy. However, the photosensitizers which can efficiently absorb NIR light are still rare. [38]

Here we have some examples of DNA photosensitizers which absorb near-infrared-light (Figure 1.7). Lu(III) texaphyrin is metal-coordinating expanded porphyrin. It is an interesting aromatic macrocycle that shows application as a photosensitizer. [39] The advantage of this photosensitizer is high light absorption around 730 nm. Remarkable properties of this agent are low systemic toxicity, preferential localization in the tumor, water solubility to enable administration in aqueous solutions and high photodynamic efficiency. [40] This photosensitizer is suitable to use for photodynamic treatment of recurrent breast cancer and light-based age-related macular degeneration, a vision-threatening disease of the retina. [41] A photocleavage reaction of Lu(III) texaphyrin showed that at 730 nm, plasmid DNA was photo-cleaved into nicked DNA in 93% yield when irradiated for 60 min. In order to have more penetration of light, the possibility of utilizing lutetium(III) texaphyrin as a near-infrared PDT photosensitizing agent

was therefore explored. [17] vanadium(IV) complex based on curcumin, which is extracted from *Curcuma longa* Linn (turmeric), was selected because of its anti-cancer activity. It has the ability to form reactive oxygen species upon light activation. [17] [42], [43] When irradiated at 785 nm, the curcumin compound cleaves plasmid DNA in 48% yield by a hydroxyl radical pathway. Under 400–700 nm illumination, the curcumin complex was found to be significantly phototoxic in HeLa cancer (human cervical cancer cells). [17] A catechol unit was used a Fe(III) complex to achieve an intense ligand-to-metal charge transfer (LMCT) absorption band within the near-infrared PDT window. Analysis of the spectrum of this compound showed a visible band at 805 nm corresponding to the catechol–Fe(III) LMCT transition. Irradiation of 25 μ M of this complex at 785 nm for 60 min shows an 83% yield of DNA photocleavage. ROS scavenger and D₂O studies pointed to the involvement of hydroxyl radicals in the cleavage mechanism.[17]

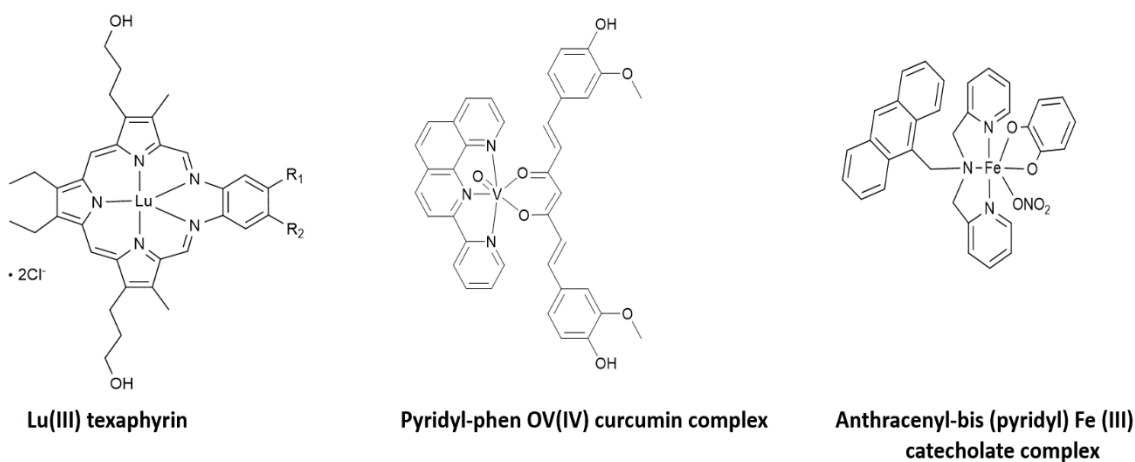


Figure 1.6 Chemical structures of photosensitizers that absorb long wavelengths of light

1.2 Summary of the research

Professor Maged Henary's lab at Georgia State University synthesized a series of quinoline polymethine cyanine dyes to achieve absorption in NIR range. Some of these cyanine dyes generate considerable damage of DNA upon irradiation with long wavelengths of light. We

decided to study the mechanisms of photocleavage by using different chemical additives. To further clarify the cause of photocleavage for these cyanine dyes we used UV-visible spectroscopy, gel electrophoresis, and other methods. The primary goal of this thesis was to elucidate the mechanism of photocleavage of DNA of dye **1** and **2**. Figure 1.7 shows the structure of dyes that have been used in our experiments. Dye **1** and **2** showed the most photocleavage activity in the NIR light range. The first section of Chapter 3 focuses on UV-visible absorbance of dye **1**, **2** and **3** under various circumstances to show us the maximum absorbance and stability of the compounds. The second section shows a series of DNA photocleavage gel electrophoresis experiments of our compounds under a different conditions such as wavelength, time, concentration and temperature. In Section 3, a photocleavage mechanism is proposed with the help of the results of scavenger reactions. Determining the mechanisms of photochemical oxidative reaction of photosensitizers in photodynamic therapy applications has been a challenging problem. A wide variety of assays are available for both singlet oxygen and hydroxyl radicals detection. In photochemical oxidations, generation of singlet-oxygen often competes with the generation of hydroxyl radical. The fraction of the photochemical oxidation by each one depends on the conditions. When the concentration of oxygen is high, generation of singlet oxygen or superoxide is high. The results of our mechanistic studies suggested that cyanine dyes **1** and **2** cleave DNA by a type 1 hydroxyl radical pathway and dye **2** cleave DNA more efficiently compare to dye **1** and **3**.

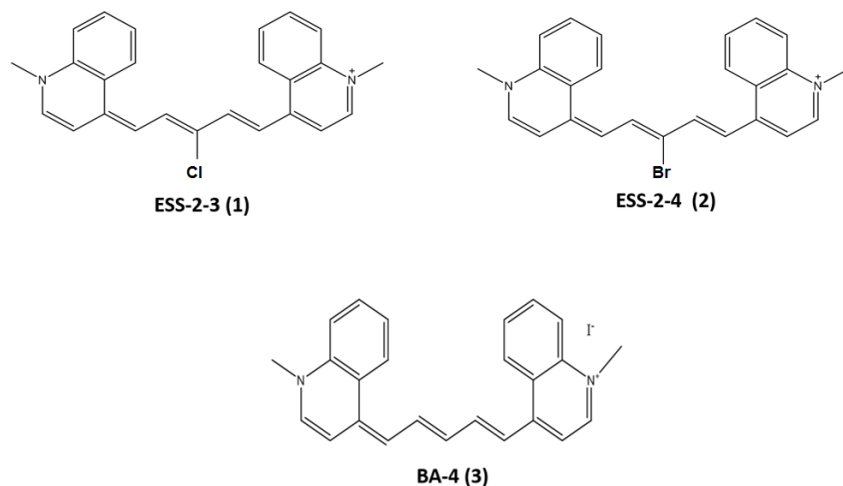


Figure 1.7 Synthesized cyanine dyes by Dr. Henary's lab at Georgia State University

2 EXPERIMENT

2.1 Materials

Deionized distilled water was used for buffer and sample preparation. Sodium phosphate buffer at pH 7.0 was prepared from sodium phosphate monobasic and sodium phosphate dibasic, Fisher Scientific (Fairlawn, NJ). DNA used for UV-visible spectrophotometry was calf thymus DNA (CT DNA), obtained from Invitrogen (Cat. No. 15633-019, 10 mg/mL, average size ≥ 2000 bp). For gel electrophoresis experiments, pUC-19 plasmid DNA was used and the concentration and purity was checked by UV-visible spectrophotometry. Standard protocols were used to transform *E. coli* competent cells (Stratagene, XL-1 blue) with pUC19 plasmid DNA (Sigma-Aldrich) and to clone the plasmid in bacterial cultures. PUC-19 purification was performed using a QIAfilter Plasmid Mega Kit (Qiagen™, Cat. No. 12263). Agarose, ethidium bromide (EtBr), dimethyl sulfoxide (DMSO) and methanol ($\geq 99.8\%$) were purchased from Sigma-Aldrich (St. Louis, MO). Photocleavage inhibition experiments were used sodium azide ($\geq 99.99\%$), sodium benzoate (99%), deuterium oxide (D₂O) and catalase from Sigma-Aldrich (Milwaukee, WI).

Amplex Red Sphingomyelinase Assay Kit (Lot. No. A22188) was from Thermo Fisher Scientific for hydrogen peroxide detection (Carlsbad, CA). Methanol ($\geq 99.8\%$) was purchased from Sigma-Aldrich (St. Louis, MO). Electrophoresis loading buffer was 15.0% (w/v) ficoll and 0.025% (w/v) bromophenol blue. The cyanine dyes in this research were synthesized by Dr. Henary's laboratory at Georgia State University and were stored in -4°C freezer as concentrated stock solutions in dimethyl sulfoxide (DMSO, $\geq 99.99\%$) from Sigma-Aldrich (St. Louis, MO).

2.2 Instruments

The light emitting diode (LED) lasers were utilized as light sources in all cleavage experiments were dot shaped from Laser Land Company, with peak emission wavelengths of 808 nm (300 mW), 830 nm (300 mW) and 850 nm (100 mW). Low-intensity light emitting diodes, at 850 nm were being used as well (Environment lights.com). UV-visible spectra were obtained with a PerkinElmer Lambda 35 spectrophotometer and the graphs of the spectra were plotted via Microsoft Office Excel. Circular dichroism (CD) and induced circular dichroism (ICD) spectra were acquired using a Jasco J-810 spectropolarimeter. Agarose gels were electrophoresed with a gel electrophoresis box from Bio-Rad Laboratories. Gels were stained with ethidium bromide (5 mg/mL in H_2O). Electrophoresed gels were visualized by transilluminator (VWR Scientific, LM-20E) at 302 nm, and then photographed with a UVP PhotoDoc-It™ imaging system. For quantitating the gels, the ImageQuant version 5.2 software was employed. Fluorescence spectra were recorded with an RF-1501 spectrofluorometer (Shimadzu Scientific Instruments).

2.3 Method

2.3.1 *UV-visible absorption*

The absorbance of the prepared cuvettes containing compounds was tested using a UV-visible spectrophotometer in the wavelength range from 1100 nm to 200 nm. In time course measurements, absorbance was recorded every 5 min from $t=0$ to $t=30$ min until the absorption of the solution did not change. Cuvettes contained 10 μM of compound in DMSO without CT DNA or 10 mM of sodium phosphate buffer (pH 7.0) in presence and absence of the CT-DNA. The volume in each cuvette was 500 μL . In CT-DNA titration experiments, small volumes of an aqueous stock solution of CT-DNA were sequentially added to samples containing 10 μM of dye **1** or **2** in the presence of 10 mM of sodium phosphate buffer pH 7.0.

2.3.2 *Preparation of agarose gel*

For making a 1.5% gel, 1.5 g agarose was dissolved in 100 mL 1X TAE buffer. The mixture was heated to a molten state in a microwave, and then 5 μL of ethidium bromide (5 mg/mL in H_2O) was added. The liquid gel was poured into a tray. When the gel solidified, we put it in the gel box and filled it with 1X TAE running buffer. A total of 20 μL of the previously prepared photocleavage samples were loaded into the wells and 40 μL of ethidium bromide (5 mg/mL) was added to the running buffer.

2.3.3 *Preparation of sodium phosphate buffer and samples*

The phosphate buffer was prepared from 1.0 M solutions of mono and dibasic sodium phosphate. In order to prepare the monobasic salt, 35.49 g NaH_2PO_4 was dissolved in 250 mL DI H_2O . The same amount of dibasic salt was also dissolved in 250 mL dd H_2O . Both monobasic and dibasic sodium phosphate solutions were diluted in dd H_2O to a total volume of

1000 mL by combining 57.7 mL of Na_2HPO_4 and 42.3 mL of Na_2HPO_4 . The pH was adjusted to 7.0 using 50% NaOH (Fisher Scientific).

Photocleavage samples were prepared as follows. The total volume of each sample was 40 μL . The solutions order of the reagent, and the final concentrations of each reagent are listed below.

ddH₂O
10 mM Sodium phosphate buffer (pH 7.0)
38 μM bp pUC19
20 μM Dye

2.3.4 *Plasmid DNA photocleavage*

Tubes containing 40 μL of our reaction mixture consisting of 20 μM cyanine dyes **1**, **2** and **3**, 38 μM bp pUC-19 plasmid DNA and 10 mM sodium phosphate buffer (pH 7.0) were irradiated with an 808 nm, 830 nm or 850 nm laser for 30 min. Then, 3 μL of electrophoresis loading buffer (15.0% (w/v) Ficoll, 0.025% (w/v) bromophenol blue) was added to the reaction mixture. A total of 20 μL was loaded into the well of the 1.5% non-denaturing agarose gel stained with ethidium bromide (5 mg/mL). Gel electrophoresis was conducted at 105 V in 1 \times TAE buffer (tris-acetate-EDTA) for about 60 min. During the electrophoresis, molecules migrate towards the opposite charge. A molecule with a negative charge will be pulled to the positive end (opposites attract!). DNA is negatively charged. Therefore, when an electric current is applied to the gel, the DNA will migrate to the positively charged electrode. Molecules are separated by their size and charge. Smaller molecules migrate through the gel more quickly and therefore travel further than larger fragments. We visualize the gels using ultraviolet transilluminator at 302 nm which will show the EtBr stained as a bright fluorescent bands and take a picture of the gel via photography.

2.3.5 DNA photocleavage time course experiments

A series of 20 μ L reactions was prepared containing 38 μ M bp pUC19 DNA, 10 mM sodium phosphate buffer pH 7.0, and 20 μ M concentrations of dye **1** or **2**. The samples were irradiated at 808 nm and 830 nm for time periods from 5 to 120 min in 20 min increments at room temperature in Eppendorf tubes. Reaction products were resolved on a 1.5 % non-denaturing agarose gel and quantitated with Gel Quant 5.2 software. Table 1 shows the reaction content of time course profile experiments with dye **1** and **2**.

Table 1. Time course analysis reaction conditions

Concentration (μ M)	1	2	3	4	5	6	7	8
Buffer	10 mM	10 mM	10 mM	10 mM	10 mM	10 mM	10 mM	10 mM
pUC-19	38 μ M bp	38 μ M bp	38 μ M bp	38 μ M bp	38 μ M bp	38 μ M bp	38 μ M bp	38 μ M bp
Dye	20 μ M	20 μ M	20 μ M	20 μ M	20 μ M	20 μ M	20 μ M	20 μ M
Light (min)	5	10	20	40	60	80	100	120

2.3.6 Fluorescence spectroscopy

To uncover the mechanism of photocleavage for our compounds, a fluorimeter was used to detect H_2O_2 using an Amplex Red reaction. Amplex® Red reagent is a colorless substrate that reacts with hydrogen peroxide (H_2O_2) to produce highly fluorescent resorufin (excitation= 563 nm; emission= 587 nm).[44], [45] In the presence of peroxidase enzyme, Amplex Red reacts with H_2O_2 in a 1:1 stoichiometry to produce the resorufin, a red fluorescent compound (Figure 2.1). Resorufin has an absorption and fluorescence emission maxima of 563 nm and 587 nm, respectively. Amplex® Red reagent is a fluorogenic substrate that has minimum background fluorescence.

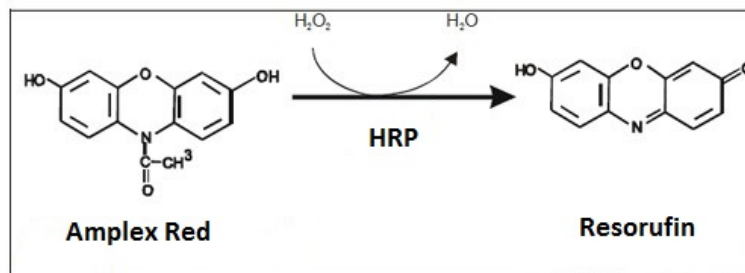


Figure 2.1 Conversion of Amplex Red into Resorufin

Amplex Red reagents came from the Thermo Fisher Scientific Amplex Red Sphingomyelinase Assay Kit. According to the assay kit instructions, several stock solutions were prepared. A 10 mM stock solution of Amplex Red was made by dissolving Amplex Red reagent in dimethyl sulfoxide (DMSO). Reaction buffer (1X) was comprised of 0.05 M sodium phosphate (pH 7.4) and was prepared from a 5X concentrate supplied by the kit. Horseradish Peroxidase (HRP) stock solution (10 U/ml) was prepared by dissolving HRP powder in 1X reaction buffer. Using the supplied ~3% H₂O₂ solution, a 20 mM working solution was made using (1X) reaction buffer as the diluent. A series of dilutions of hydrogen peroxide were made using the 1X reaction buffer as the diluent. In our experiment, a tube containing 40 μL of our reaction mixture (20 μM cyanine dye, 38 μM bp pUC-19 plasmid DNA, and 10 mM sodium phosphate buffer pH 7.0), were irradiated at 830 nm for 30 min. Then 260 μL of Amplex Red cocktail containing 100 μM Amplex Red and 2 U/mL horseradish peroxidase in 50 mM sodium phosphate buffer was added to each reaction. A total of 350 μL of each reaction was then diluted in a cuvette with 50 mM sodium phosphate buffer pH 7.0 to a total volume of 3000 μL. The second set of reactions was carried out in which 50 mM sodium phosphate buffer pH 7.0 was added to the initial reactions in place of the Amplex Red/HRP solution. Positive control samples were conducted using varying concentrations of hydrogen peroxide in the initial reactions. Fluorimeter slit width was set to 4.5 mm and the excitation wavelength was 550 nm.

2.3.7 Circular dichroism

Circular Dichroism (CD) is a technique for assessing DNA-binding modes. Circular Dichroism is the difference in the absorption (or emission) of left and right circularly polarized light. [46]. This technique is used for studying chiral molecules of all types and sizes. [47] Despite the ease of measurement, CD is often used in structural analysis of biological systems. [48] CD is a much less difficult technique regarding both sample consumption and time requirements. Furthermore, CD allows one to monitor the binding process in different experimental conditions easily and investigate the dynamics of the binding process. [49] In our experiments, individual samples contained 10 mM sodium phosphate buffer pH 7.0 in the presence of 10 μ M of dye **1** or dye **2**, 120 μ M of CT-DNA and a total volume of 3000 μ L. Spectra were collected using 3 mL (1.0 cm) quartz cuvettes. The following parameters were employed in the CD spectrometer: twelve acquisitions averaged scan speed, 100 nm/min; response time, 2 seconds; bandwidth, 0.5 nm.

2.3.8 Binding constant

The binding constant (K_b) is a measure of the dye–DNA complex stability. In order to estimate the binding constant of dyes **1** and **2**, the titration data were fit to absorption model of Meehan and coworkers. [50] The intense absorption spectral band around 550 nm recorded for dye **1** and **2**. K_b was calculated as an equilibrium constant for the molecule–DNA complex formation by the following formula:

$$DNA / (\epsilon_a - \epsilon_f) = [DNA] / (\epsilon_b - \epsilon_f) + 1 / K_b (\epsilon_b - \epsilon_f)$$

Where [DNA] is the concentration of DNA in base-pairs, ϵ_a is the apparent extinction coefficient calculated as $A_{obs} / [complex]$, ϵ_f corresponds to the extinction coefficient of the complex in its free form, and ϵ_b refers to the extinction coefficient of the complex in the bound

form. When we fit the data into the above equation, it gave us a straight line with a slope of $1/(\epsilon_b - \epsilon_f)$ and a y-intercept of $1/K_b(\epsilon_b - \epsilon_f)$. K_b was determined from the ratio of the slope to the intercept. [50] The experimental determination of the binding constant of a cyanine dye for its target is considerable importance. The association of **1** and **2** with DNA was studied by CT-DNA titration using UV-Vis spectrometry. Binding constants (K_b) were calculated from changes in absorbance of cyanine dyes. Figures 3.24 and 3.25 show the binding constant of three trials of Cl and Br compounds **1** and **2**.

2.3.9 Anaerobic photocleavage of plasmid DNA

Among the various devices that allow the operator to realize that conditions are characterizing strictly anaerobic techniques, an anaerobic glove box is a simple and rather obvious design that has been utilized by many workers. [51] Anaerobic chambers are used to provide an oxygen-free atmosphere for work with oxygen sensitive materials and is created by running the reaction in the presence of argon. A glove box provides a space that is completely segregated from the outside, and it is designed to maintain its inside with an artificial atmosphere, typically pure nitrogen or pure argon. It is used to protect the experiment from unwanted reaction with oxygen. The glove box system works by the principle of gas circulation: the working gas permanently circulates between the glove box and the gas purifier. The gas purification system removes oxygen from the inert gas glove box atmosphere.

During the initial setup of the chamber, air contained in the chamber must be vacuumed and replaced with argon several times. Repeating the gas exchange method in a rigid chamber increases the effect of initial removal of air. All DI water and buffers were bubbled with argon using the gas bubbler to exclude air from the reaction solvents. Preparing the sample mixtures was done in the glove box filled with argon, under the anaerobic conditions. The irradiation time

was 30 min. After 30 min, we ran the gel electrophoresis to see the effect of anaerobic irradiation compare to irradiation in air.

2.3.10 Singlet oxygen and hydroxyl radical generators

Sodium azide and sodium benzoate were used to determine the presence of singlet oxygen and hydroxyl radicals. Azide acting as a natural scavenger reacts with $^1\text{O}_2$ to give a reactive azide radical. [52] Reaction mixtures were 40 μL total volume, containing 10 mM of sodium phosphate buffer pH 7.0, 38 μM bp pUC19 plasmid DNA and 20 μM of cyanine dyes **1** and **2**, were prepared in the presence and absence of 100 mM of the singlet oxygen scavenger sodium azide or 100 mM of the hydroxyl radical scavenger sodium benzoate. Negative controls contained no dye. Reactions were irradiated for 60 min at room temperature. We removed the samples from irradiation and 3 μL 6x loading buffer were added to each tube. Then, 20 μL of each sample were loaded into the wells of a 1.5% non-denaturing agarose gel containing 5 μL of 5 mg/mL ethidium bromide in 650 mL TAE buffer with 40 μL 5 mg/mL ethidium bromide. Gels were run for 60 min at 100 V and photographed under 302 nm light. The gel images were quantitated with ImageQuant 5.2 software. The percent inhibition of DNA photocleavage was then calculated using this formula:

$$\text{Percent of Photocleavage Inhibition} = \left[\left(\frac{\% \text{ Total of Linear and Nicked DNA}_{\text{without scavenger}}}{\% \text{ Total of Linear and Nicked DNA}_{\text{with scavenger}}} \right) - \left(\frac{\% \text{ Total of Linear and Nicked DNA}_{\text{without scavenger}}}{\% \text{ Total of Linear and Nicked DNA}_{\text{without scavenger}}} \right) \right] \times 100. [7]$$

3 RESULTS AND DISCUSSION

3.1 UV-Visible absorption analysis of cyanine dyes

3.1.1 Time course UV-visible absorption study for dyes

UV-visible spectrometry was used to determine the stability of the dyes in aqueous solution and DMSO. The spectra show that all three compounds are stable in DMSO since the absorption does not change with time from 0 min to 30 min (Figure 3.1). Superimposing the compounds **1**, **2** and **3** spectra in one plot shows that the λ_{max} value of the cyanine dyes **1**, **2** and **3** are 800 nm, 795 nm, and 826 nm respectively. In 10 mM sodium phosphate buffer pH 7.0, it appears that both dye **1** and **2** undergo some degradation, while dye **3** is very unstable by comparison. (Figure 3.3) When DNA was added to 10 mM sodium phosphate buffer pH 7.0, the absorption was higher in the presence of DNA compare to absorption in the absence of DNA. (Figure 3.2) All three compounds displayed better stability in the presence of DNA, compound **1** and **2** were completely stable while compound **3** still degraded. The absorbance was collected every 5 min until the changes in absorbance were negligible.

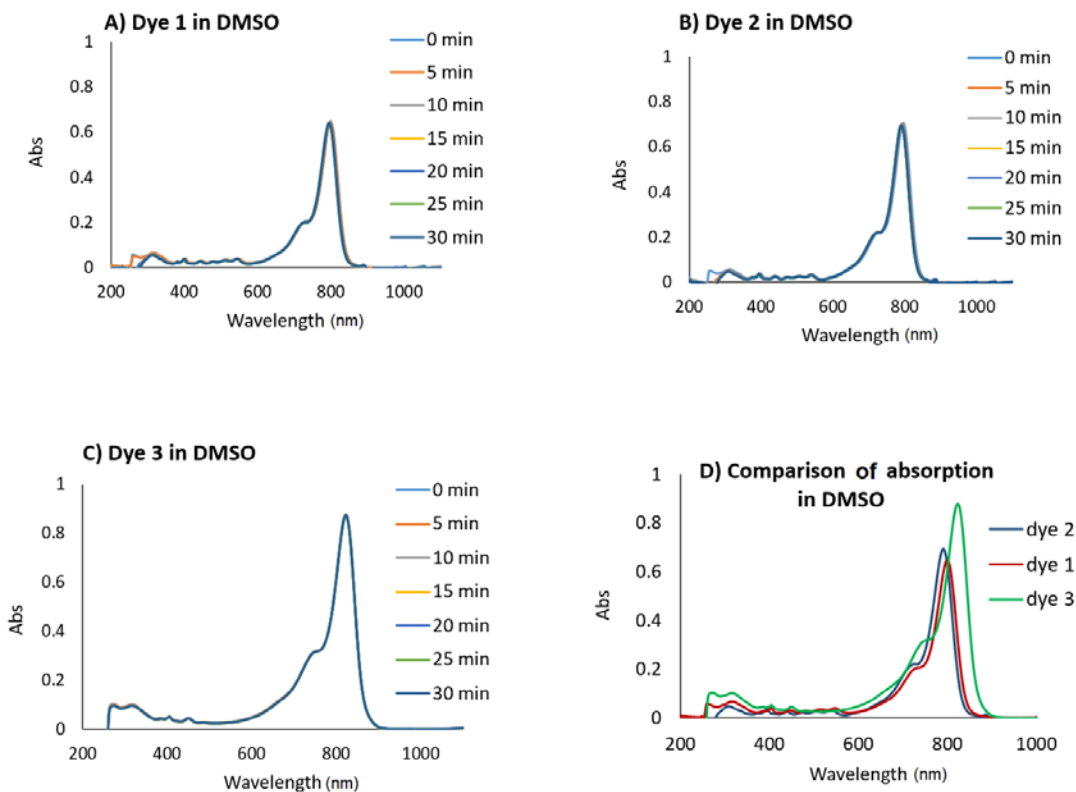


Figure 3.1 Time course UV-visible absorption spectra of cyanine 1, 2 and 3 in DMSO. Individual samples contained 10 μ M of dye in DMSO.

Figure 3.2 shows the time course UV-visible absorption of dye **1**, **2** and **3** at the first time point ($t=0$). Compound **3** shows significant decrease in the absorption in the presence of DNA compare to dyes **1** and **2**.

The spectra of compounds in the presence of DNA were used to determine initial choice of light wavelengths used in the DNA photocleavage assays. Initial testing used light closest to the wavelength at peak absorbance.

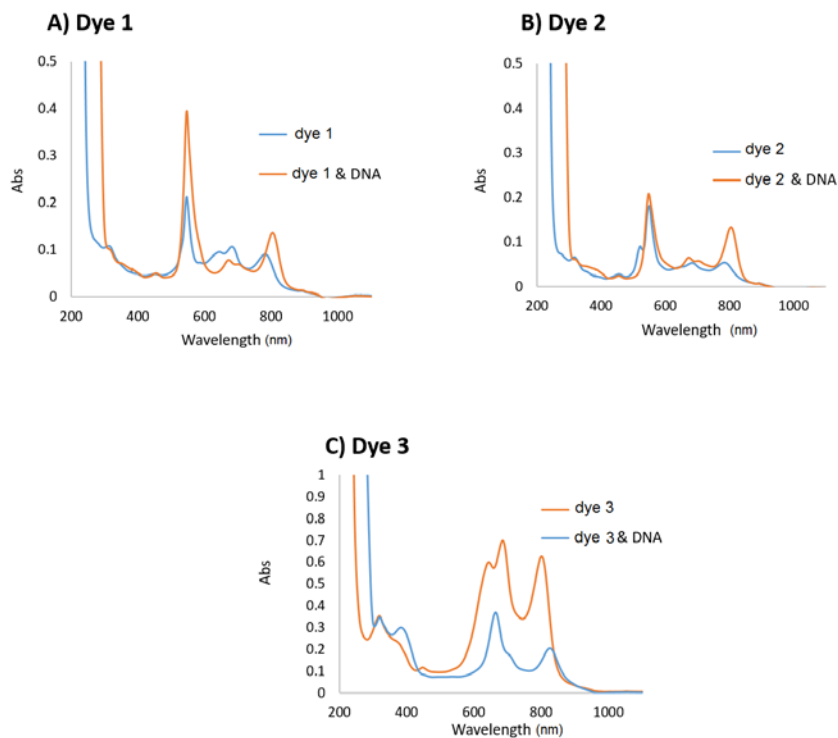


Figure 3.2 Absorption spectra upon adding calf thymus DNA. Spectral changes indicate DNA binding for A) compound 1, B) compound 2 and C) compound 3. Individual samples contain 10 μ M of A) dye 1, B) dye 2 and C) dye 3 in the presence of 150 μ M bp of calf thymus DNA and 10 mM of sodium phosphate buffer pH 7.0.

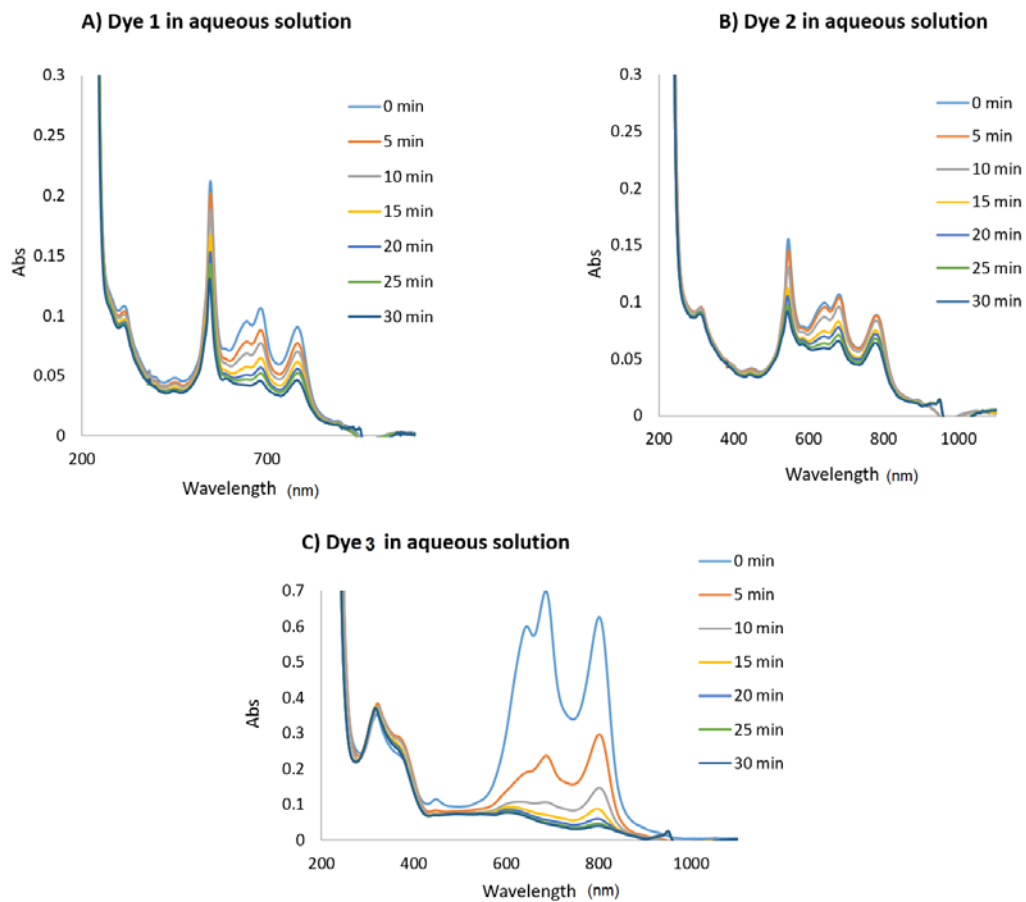


Figure 3.3 Time course UV-visible absorption study in the absence of CT-DNA. Individual samples contained 10 μ M of dyes 1, 2 and 3 in 10 mM of sodium phosphate buffer pH 7.0.

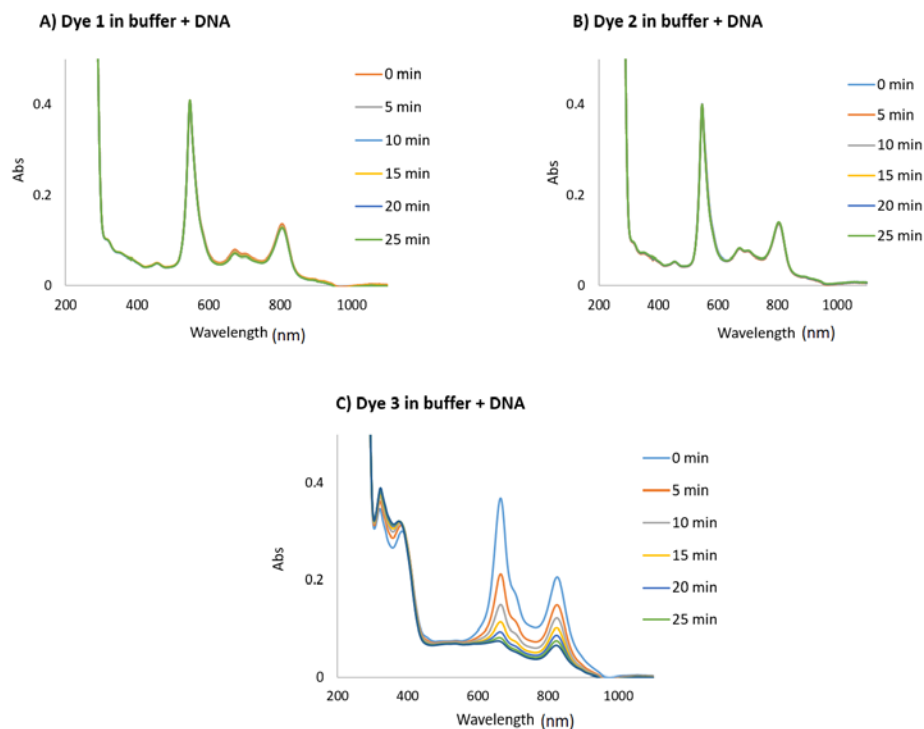


Figure 3.4 Time course UV-visible absorption study in the presence of CT-DNA. Spectra were recorded at 0, 5, 10, 15, 20 and 25 min time intervals. Individual samples contain 10 μ M of dyes 1, 2 and 3 in the presence of 150 μ M bp of CT DNA in 10 mM of sodium phosphate buffer pH 7.0.

Based on the results in Figures 3.2, 3.3 and 3.4, compound **3** is not stable in sodium phosphate buffer in the presence and absence of DNA. So, we are primarily analyzing and discussing the data from compounds **1** and **2** in the thesis, which are considerably more stable than **3** especially when DNA is present.

3.2 PUC19 plasmid DNA cleavage analysis

3.2.1 Photocleavage of supercoiled plasmid DNA at 808 nm, 830 nm, 850 nm

We first examined the photocleavage abilities of compounds **1**, **2**, and **3** toward supercoiled pUC19 plasmid DNA using gel electrophoresis. To examine the photocleavage activity of cyanine dyes **1**, **2**, and **3** we used 808 nm, 830 nm, and 850 nm lasers. Reactions consisted of 20 μ M of dye, 38 μ M bp pUC19 plasmid DNA and 10 mM sodium phosphate

buffer pH 7.0. Gel results show that cyanine dyes **1** and **2** are able to cleave DNA at these three wavelengths. Dye **3** which is unstable, was being used in gel electrophoresis as a control. (Figure 3.5 and 3.6) The photo conversion of supercoiled plasmid to its nicked and linear forms was then visualized on 1.5 % nondenaturing agarose gels. As shown in the Figure 3.5, compounds **1** and **2** cleaved DNA efficiently upon irradiation at 808 nm as indicated by the remarkable transformation of pUC19 DNA from the supercoiled form to the nicked form (lanes 7 and 8). Upon irradiation with lasers or LEDs, irrespective of the light source, the halogenated forms (Cl and Br) of the carbocyanine dyes consistently produced more photocleavage than their non-halogenated counterpart **3**. Thus, under the same conditions, the negligible DNA cleavage was observed for dye **3**, suggesting that decomposition of dye **3** in DNA and buffer solutions contributed to low cleavage yields. (Figure 3.5 and 3.6) There is a possibility that the halogenated cyanine dyes have greater propensity to bind to DNA because they are more stable compared to **3**. In addition, Br and Cl might be participating in the generation of reactive oxygen species (ROS) by the “heavy atom effect”. The “heavy atom effect” is an enhancement of the rate of a spin-forbidden transitions due to the presence of an atom of high atomic number, which is either part of, or external to, the excited molecular entity. Mechanistically, it corresponds to a spin-orbit coupling enhancement produced by a heavy atom. [53], [54] This is proposed to increase the level of cleavage by increasing triplet state cyanine dye population and the subsequent of formation of DNA damaging by reactive oxygen species.

Figure 3.5 shows that photocleavage levels were also low for plasmid DNA irradiated in the absence of dye (lane 5) and in dark control reactions (Lanes 1 to 4). It is worth emphasizing that halogen substitution is crucial for DNA photocleavage. Without irradiation, compounds **1**, **2** and **3** do not have DNA cleavage abilities.

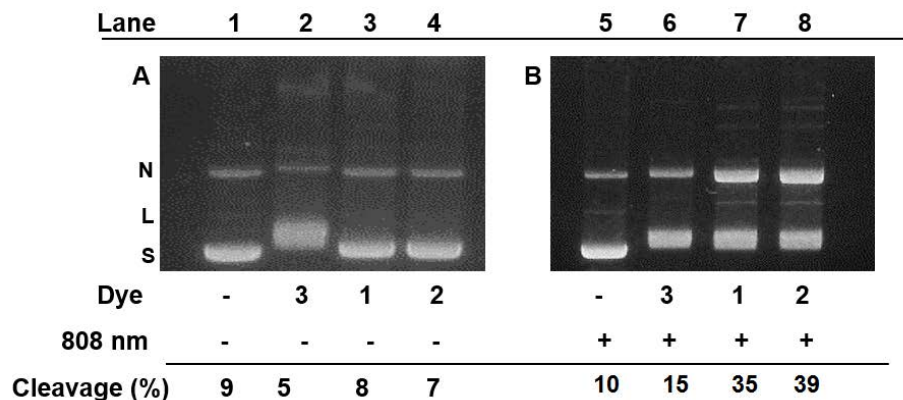
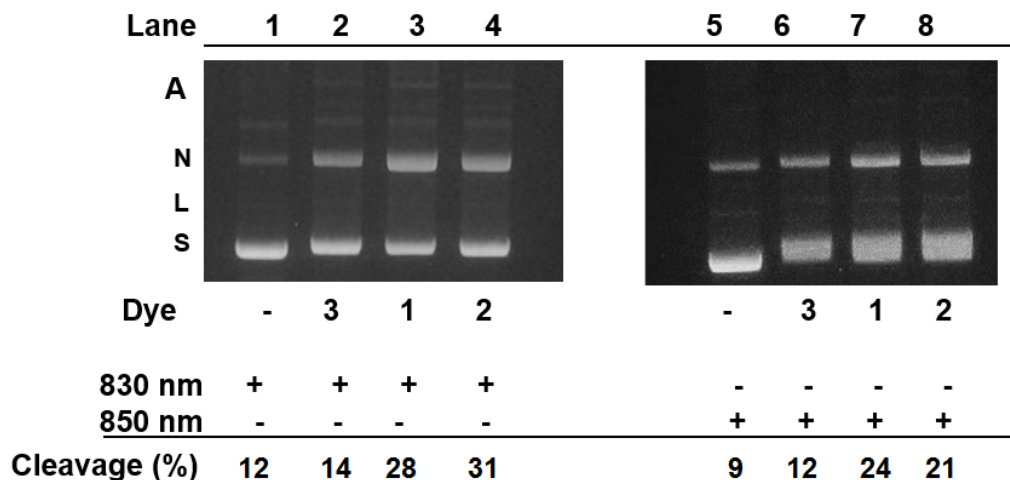


Figure 3.5 Agarose gel electrophoresis of supercoiled pUC19 plasmid DNA with an 808 nm laser.

Samples contained 20 μ M of the compound, 38 μ M bp pUC19 and 10 mM sodium phosphate buffer pH 7.0, when A contains dark controls and B shows samples irradiated for 30 min with 300 mW, 808 nm LED laser at room temperature inside a metal block. Lanes 1 to 4, dark controls. Lane 5, DNA alone; lane 6, DNA + dye 3, lane 7, DNA + dye 1; lane 8, DNA + dye 2. S and N denote supercoiled circular and nicked-circular plasmid forms, respectively.

DNA photocleavage by **1**, **2**, and **3** is observed upon irradiation at 808 nm, 830 nm and 850 nm. (Figure 3.6) We kept the temperature constant at 22 $^{\circ}$ C during the irradiation by putting the sample tubes in a metal block. Metal blocks are heat conductors, so they transfer the heat from samples during the irradiation into the metal block. A thermometer inside the metal block showed that the temperature was 22 $^{\circ}$ C. We also use a cooling fan during irradiation to make sure the temperature of samples did not increase.



*Figure 3.6 Agarose gel electrophoresis of supercoiled pUC19 plasmid DNA. Samples contained 20 μ M of compounds, 38 μ M base pair of pUC19 and 10 mM sodium phosphate buffer pH 7.0, upon irradiation with **A**) an 830 nm laser, 300 mW and **B**) an 850 nm laser, 100 mW for 30 min at room temperature inside the metal block. Temperature was measured with a thermometer and maintained at 22 $^{\circ}$ C. Lane 1 and 5, DNA alone; lane 2 and 6, DNA + dye 3, lane 3 and 7, DNA + dye 1; lane 4 and 8, DNA + dye 2. S and N denote supercoiled circular and nicked-circular plasmid forms, respectively.*

Based on the results from the gel pictures in Figures 3.5 and 3.6, the percentage of cleavage of DNA at 808 nm and 830 nm is more than at 850 nm for both compounds 1 and 2, reflecting lower light absorption at 850 nm and the lower power of the 100 mW, 850 nm laser.

3.2.2 Temperature-dependent experiments

The goal of these series of experiments was to determine if any heat generated by the 808 nm, 830 nm and 850 nm lasers might be responsible for DNA cleavage by the cyanine dyes. To address this concern, dark control temperature-dependent experiments were designed at 10 $^{\circ}$ C, 22 $^{\circ}$ C, and 37 $^{\circ}$ C. Samples were run inside the metal block. The temperature of the reactions was carefully monitored by a thermometer. For the low temperature experiment, we put the metal block in an ice container and put the samples and thermometer inside the block. When we wanted to run our experiment at 37 $^{\circ}$ C, we put the samples inside the metal block with a

thermometer inside the block and set the temperature of the block at 37 °C using a heater. If we were to get cleavage in the dark at 37 °C, this would suggest that the compounds might have thermal activity as well. Based on the results from the gel picture in Figure 3.7, the compounds showed equivalent low background levels of thermal cleavage at 37 °C compared to 10 °C and 22 °C. This suggests the photocleavage is not related to temperature (thermal cleavage) and the photocleavage may be because of the intrinsic photoactivity of the cyanine dyes.

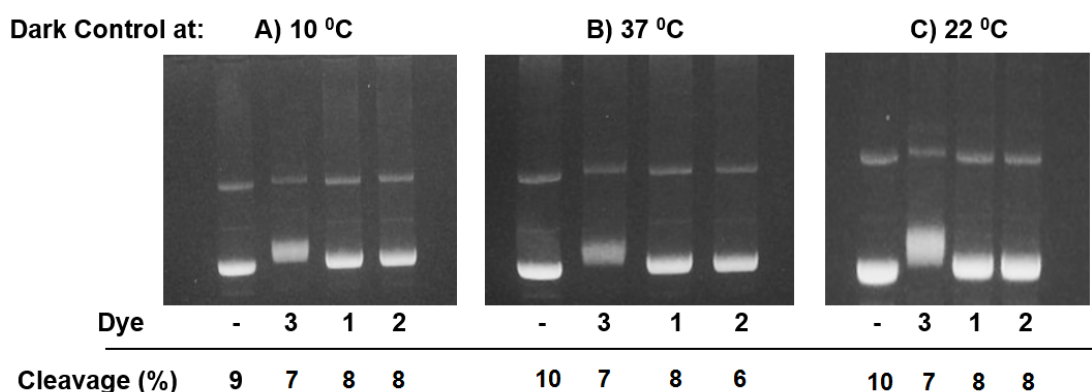


Figure 3.7 Dark control reactions.

*A photograph of a 1.5 % non-denaturing agarose gel showing photocleavage of 38 μ M bp of pUC19 plasmid DNA in the presence of 20 μ M of dye, 10 mM sodium phosphate buffer pH 7, being kept in the dark for 30 min. **A)** Dark control at 10 °C, **B)** Dark control at 37 °C, **C)** Dark control at 22 °C*

In order to examine the effect of possible heat production of long wavelength lasers, the photocleavage experiments in an ice container at 10 °C where irradiated with 808 nm, 830 nm and 850 nm lasers and compared to the cleavage at room temperature. All of the resulting cleavage yields were similar, suggesting that DNA photocleavage by dyes **1**, **2** and **3** was not entirely due to heat generated by the lasers. (Figure 3.8, 3.9, 3.10)

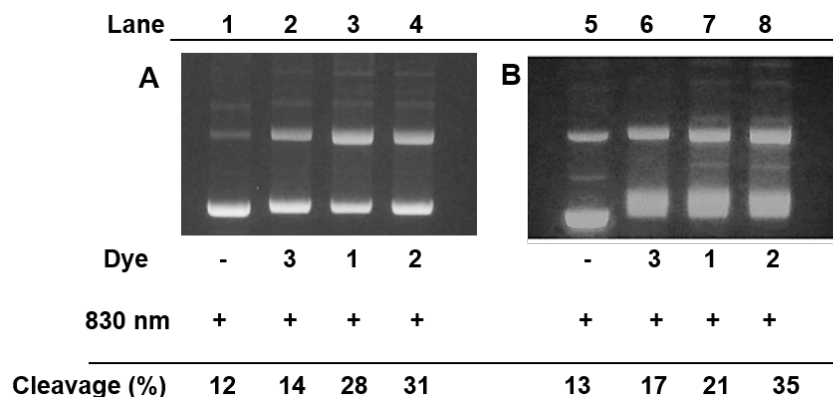


Figure 3.8 Temperature dependent experiment at 830 nm, 300 mW.

A) Experiment run at 22 °C, B) Experiment run at 10 °C. Agarose gel electrophoresis of supercoiled pUC19 plasmid DNA (38 μM base pair) in the presence of 20 μM of dye 1, 2 and 3 and 10 mM sodium phosphate buffer pH 7.0, upon irradiation with 830 nm laser, 300 mW at 10 °C for 30 min. In **B** samples were irradiated in a metal block inside an ice container to remove heat for 30 min. Temperature was measured with a thermometer and maintained at 10 °C.

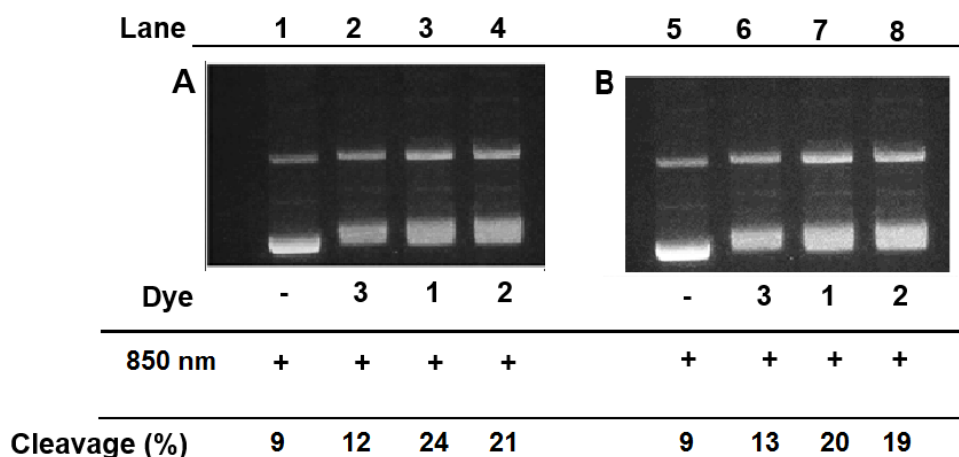


Figure 3.9 Temperature dependent experiment at 850 nm 100 mW.

A) Experiment run at 22 °C, B) Experiment run at 10 °C. Gel electrophoresis of compounds 1, 2 and 3 with 850 nm laser, 100 mW. Samples contained 38 μM bp of pUC19 plasmid DNA, 20 μM of dyes, 10 mM of sodium phosphate buffer pH 7.0 irradiated with 850 nm laser, 100 mW at ice container at 10 °C for 30 min. In **B** samples were irradiated in a metal block inside an ice container to remove heat for 30 min. Temperature was measured with a thermometer and maintained at 10 °C.

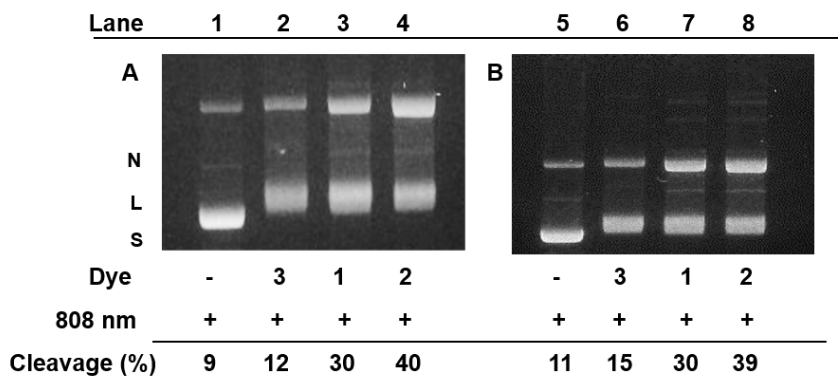


Figure 3.10 Temperature dependent experiment at 808 nm.

Gel electrophoresis of compounds 1, 2 and 3 with 808 nm laser, 300 mW at 10 °C. A) Experiment is run at 10 °C and B) Experiment is run at 22 °C. Samples contained 38 μM bp of pUC19 plasmid DNA, 20 μM of dyes, 10 mM of sodium phosphate buffer pH 7.0 irradiated with 808 nm laser, 300 mW at ice container at 10 °C for 30 min. In B samples were irradiated in a metal block inside an ice container to remove heat for 30 min. Temperature was measured with a thermometer and maintained at 10 °C.

3.2.3 Time course photocleavage

Cyanine dyes have been investigated for use as DNA photosensitizers, and based on our experiments, a considerable amount of supercoiled DNA was nicked using long wavelength light generated by 808, 830 and 850 nm lasers. The goal of our next experiment was to quantitate the amounts of DNA photocleavage produced by cyanine dye **1** and **2** as a function of time to determine the best reaction times for future studies. Figures 3.11 and 3.12 show the photo activity of cyanine dyes **1** and **2** upon irradiation with 830 nm laser, 300 mW up to 120 min at 22 °C, in which a large amount of nicked and even linear DNA were produced. Based on the results from the gel pictures in Figure 3.11, large amount of DNA cleavage appear after only 5 min. After that time point, changes in photocleavage were not statistically significant. So 5 min is the best reaction time for photocleavage activity evaluation for compounds **1** and **2**, because of the generation of sufficient broken DNA.

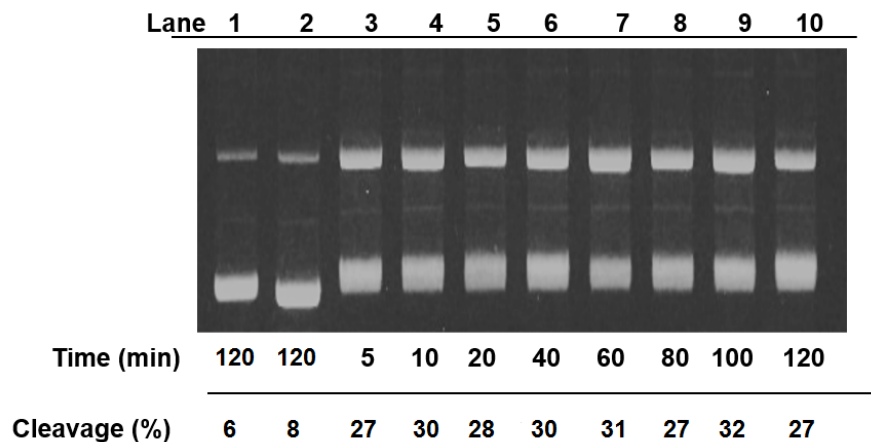


Figure 3.11 Time course experiment for dye 1.

Photographs of 1.5 % non-denaturing agarose gel showing DNA photocleavage by cyanine dye 1 at 5, 10, 20, 40, 60, 80, 100 and 120 min time intervals. Each of the samples was prepared in the presence of 20 μ M compound, 10 mM sodium phosphate buffer pH 7.0, and 38 μ M bp pUC19 DNA, in a 20 μ L reaction volume. Lane 1 and 2 are respectively dark (with compound) and light (without compound) controls. Samples were irradiated with a 300 mW, 830 nm laser in a metal block to remove heat for 30 min. Temperature was measured with a thermometer and maintained at 22^o C.

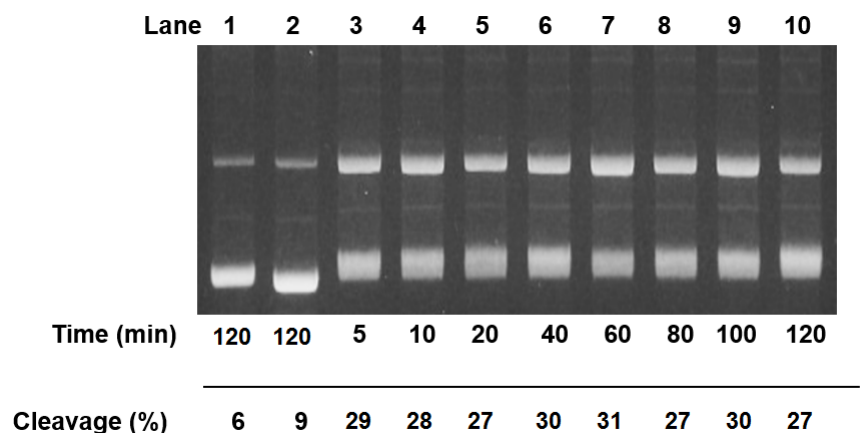


Figure 3.12 Time course experiment for dye 2.

Photographs of 1.5 % non-denaturing agarose gels showing DNA photocleavage by cyanine dye 2 at 5, 10, 20, 40, 60, 80, 100, 120 min intervals. Each of the samples was prepared in the presence of 20 μ M compounds, 10 mM sodium phosphate buffer pH 7.0 and 38 μ M bp pUC19 DNA, in a 20 μ L reaction volume. Lane 1 and 2 respectively represent dark (with compound) and light (without compound) controls. Samples were irradiated with 300 mW, 830 nm laser in a

metal block to remove heat for 30 min. Temperature was measured with a thermometer and maintained at 22^o C.

3.2.4 Concentration titration of cyanine dyes 1 and 2

One important step for optimizing photocleavage reactions of the cyanine dyes is to evaluate the best concentration of compound in which we can get the maximum DNA photocleavage. To reach this goal, our next photocleavage experiment was conducted to evaluate the effect of increasing the concentration of compounds **1** and **2** on DNA photocleavage with fixed amount of DNA and sodium phosphate buffer pH 7.0. The concentration of dyes ranged from 5 μM to 50 μM . Parallel dark controls were prepared. The wavelength of the laser lamps was 830 nm. From the result in Figures 3.13 and 3.14, it is evident that the amounts of DNA photocleavage produced by compounds **1** and **2** increased as a function of increasing dye concentration from 5.0 μM up to 20 μM of dye. For those samples that had more than 20 μM of dye, there was not a significant increase in cleavage. This tells us that 20 μM is the best concentration for dyes **1** and **2** to photocleave DNA. These dyes displayed lower level of cleavage at concentration lower than 20 μM .

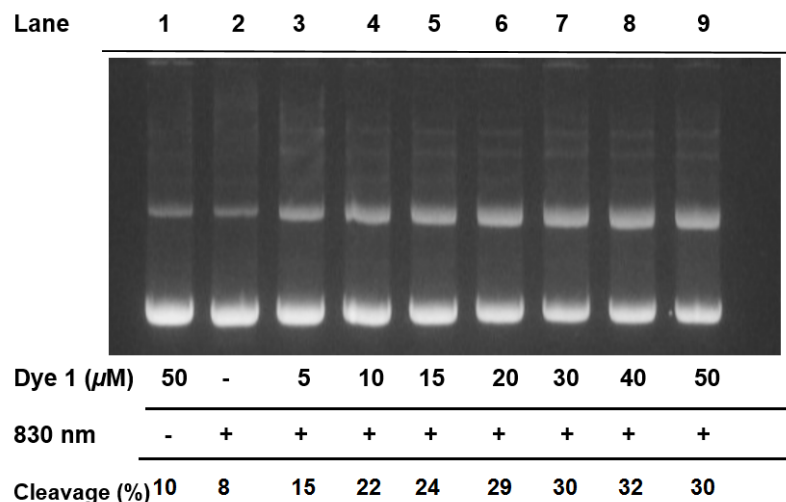


Figure 3.13 Concentration titration experiment for dye I.

Photograph of 1.5% nondenaturing agarose gel showing photocleavage of the pUC19 plasmid as a function of compound I concentration. Samples contained 10 mM sodium phosphate buffer pH 7.0 and 38 μM bp DNA 5 μM to 50 μM of dye I. Samples were irradiated with a 300 mW, 830 nm laser in a metal block to remove heat for 30 min. Temperature was measured with a thermometer and maintained at 22 $^{\circ}\text{C}$. A control reaction remained in dark for 30 min at 22 $^{\circ}\text{C}$.

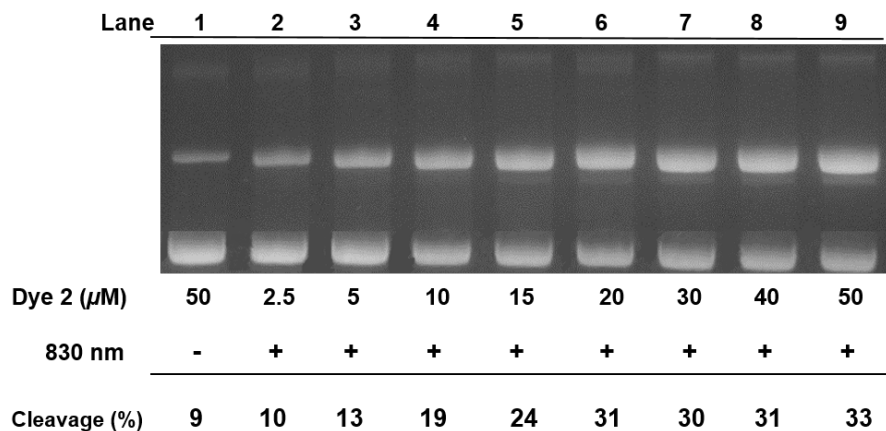


Figure 3.14 Concentration titration experiment for dye 2.

Photograph of 1.5% nondenaturing agarose gel showing photocleavage of the pUC19 plasmid as a function of compound 2 concentration. Samples contained 10 mM sodium phosphate buffer pH 7.0 and 38 μM bp DNA and 5 μM to 50 μM of dye 2. Samples were irradiated with a 300 mW, 830 nm laser in a metal block to remove heat for 30 min. Temperature was measured with a thermometer and maintained at 22 $^{\circ}\text{C}$. A control reaction remained in dark for 30 min at 22 $^{\circ}\text{C}$.

3.2.5 Photocleavage mechanism of dyes 1 and 2

The overall goal of the following experiments was to elucidate the mechanism of photocleavage by dye **1** and **2**. Castano et al. pointed out that the most important factor in PDT is understanding how the photosensitizer interacts with cells in the target tissue or tumor, and the key aspect of this interaction is the subcellular localization of the PS. [55] As we discussed previously, photosensitizers can undergo two types of photochemical reactions. In type 1 photocleavage, PS react with the tissue or molecules directly and transfer an electron or a proton to produce a radical anion or cation. When an electron is transferred to $^3\text{O}_2$, ROS are formed. In the type 2 pathway, the energy of the PS directly is transferred to molecular oxygen either from ground state or triplet state to produce excited state singlet oxygen. The two mechanism can occur simultaneously, but the ratio between these two types of reactions can be different. [55] In type 1 reactions, transferring the electron from triplet state photosensitizer to molecular oxygen causes the initial production of the superoxide anion radical. Superoxide anion does not cause

much oxidative damage in biological systems, but it can form hydrogen peroxide. [55], [56], [57] One important feature of hydrogen peroxide is, it passes through the cell membrane and when it comes into contact with Fe (II) or Cu (I), it produces the highly reactive hydroxyl radical ($\text{HO}\cdot$), a powerful biological oxidant that damage lipids, proteins and DNA. [55]. The half-life of singlet oxygen and hydroxyl radicals are short, so only those molecules close to the area of photosensitizer localization are affected. [58]

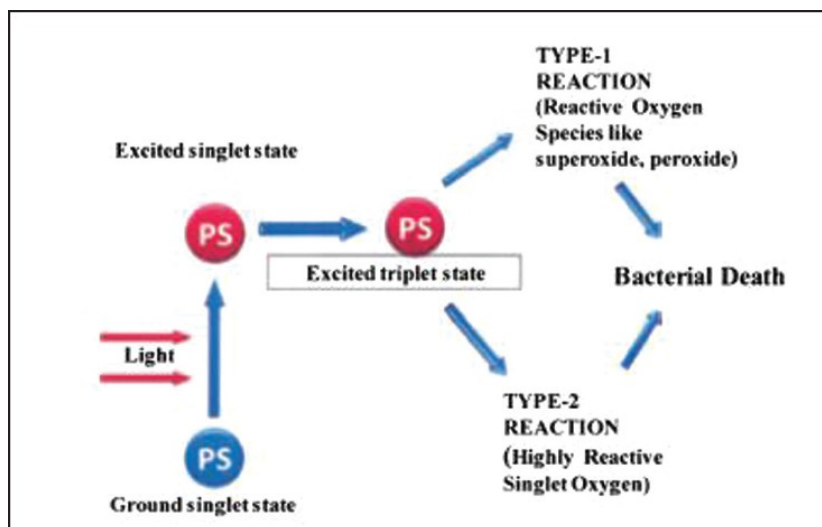


Figure 3.15 Mechanisms of action in photodynamic therapy

3.2.6 Photocleavage of pUC19 DNA, scavenger assay

To investigate the mechanism(s) involved in DNA photocleavage, we performed experiments in which DNA photocleavage reactions were done in the presence of the scavengers sodium azide for singlet oxygen ($^1\text{O}_2$), catalase for hydrogen peroxide, and sodium benzoate for the hydroxyl radical ($\cdot\text{OH}$). If the scavengers inhibit DNA damage successfully, then the quantity of supercoiled DNA should be increased, and the amount of the nicked and linear DNA should be decreased. Sodium azide and sodium benzoate produced a modest inhibitory effect, indicating that singlet oxygen and hydroxyl radicals might to some extent contribute to DNA photocleavage by dyes **1** and **2**. (Figure 3.16)

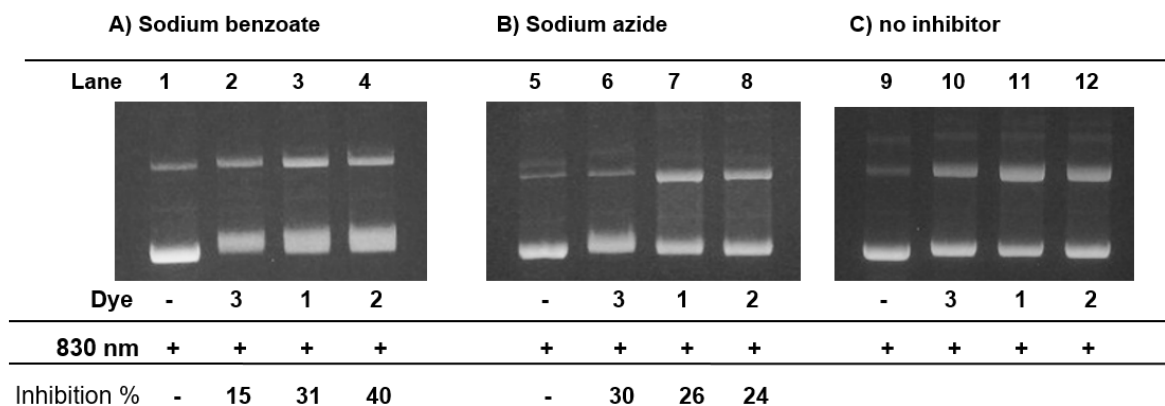
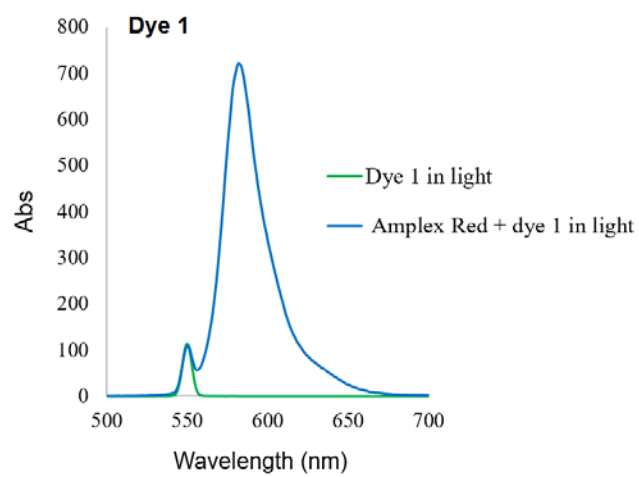
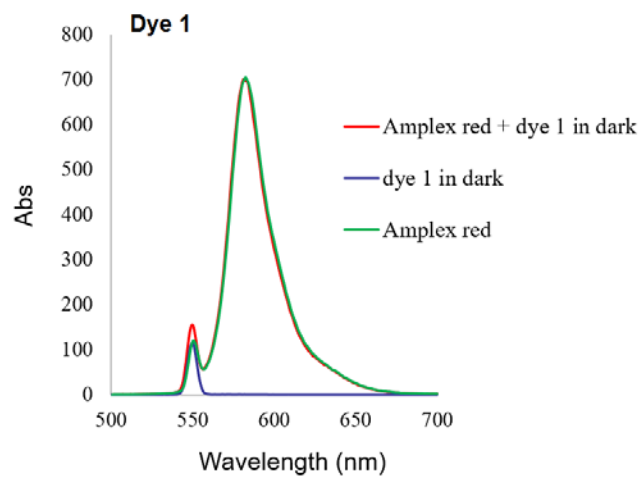


Figure 3.16 Photocleavage with scavengers sodium benzoate and sodium azide. Photocleavage inhibition reactions consisting of 38 μ M bp of pUC19 plasmid DNA were equilibrated with 20 μ M of cyanine dyes, 100 mM of scavenger sodium benzoate or sodium azide, and 10 mM sodium phosphate buffer pH 7.0. Samples were irradiated with a 300 mW, 830 nm laser in a metal block to remove heat for 30 min. Temperature was measured with a thermometer and maintained at 22 $^{\circ}$ C.

3.2.7 Hydrogen peroxide measurement using Amplex Red

As mentioned previously, type one electron transfer to oxygen produces superoxide anion radicals that form hydrogen peroxide. Using Amplex Red reagent, hydrogen peroxide can be measured in a one step process. Amplex Red, in the presence of the horse radish peroxidase enzyme, reacts with H₂O₂ in 1:1 stoichiometry to decompose H₂O₂ to hydroxyl radicals, which are reduced to water as a result of irreversible chemical oxidation of Amplex Red to resorufin. [59] Resorufin is the oxidized form of Amplex Red and produces a characteristic fluorescent signal at 585 nm. Increasing levels of H₂O₂ cause a linear increase in fluorescent product. The results in Figure 3.17 show that no H₂O₂ was detected upon treatment of complexes **1** and **2** photocleavage reaction with the Amplex red reagent. Positive controls for Amplex red detection of H₂O₂ are shown in Figure 0.2 in Appendix A.



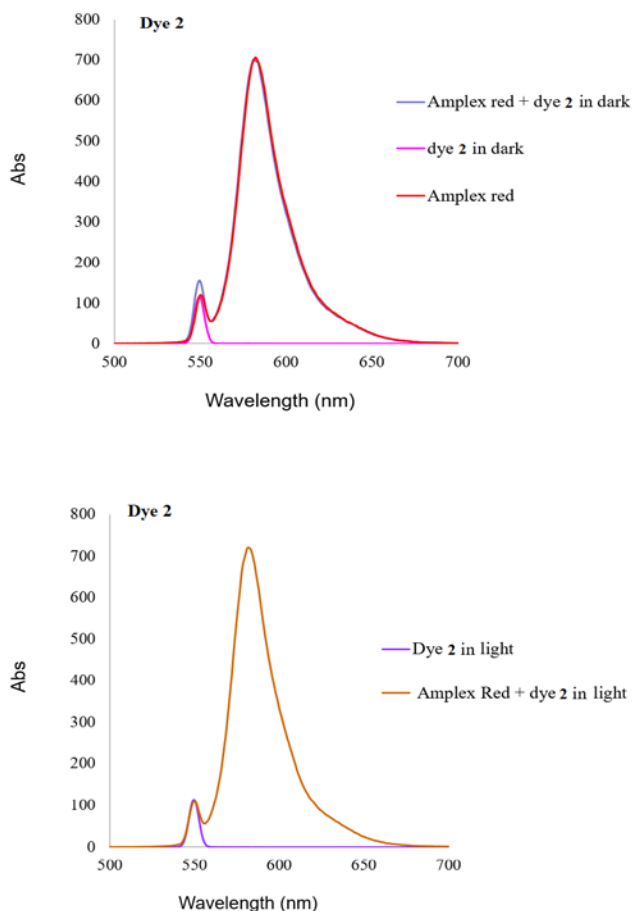


Figure 3.17 Hydrogen peroxide measurement using Amplex Red.

Samples contained 40 μL of the reaction mixture consisting of 20 μM cyanine dye, 38 μM bp pUC-19 plasmid DNA and 10 mM sodium phosphate buffer pH 7.0, irradiated with a 300 mW, 830 nm laser for 30 min at room temperature. Then 260 μL of Amplex Red cocktail containing 100 μM Amplex Red and 2 U/mL horseradish peroxidase (HRP) in 50 mM sodium phosphate buffer pH.7.0 was added to each reaction. A total of 350 μL of each reaction was then diluted in a cuvette with 50 mM sodium phosphate buffer to a total volume of 3000 μL .

3.2.8 Hydrogen peroxide scavenger, catalase

Catalase is a common enzyme found in nearly all living organisms exposed to oxygen. It catalyzes the decomposition of hydrogen peroxide to water and oxygen. It is a crucial enzyme in protecting the cell from oxidation by reactive oxygen species (ROS). The reaction will increase with the increasing enzyme concentration when the molecules of hydrogen peroxide are freely available. The more concentrated the catalase, the more chance of the molecules colliding

with the hydrogen peroxide molecules resulting in a faster reaction. In this experiment, the aim was to use catalase as an H₂O₂ scavenger to confirm the negative Amplex Red data. The gel picture in Figure 3.18 shows that catalase did not inhibit DNA photocleavage by **1** and **2**. Taken together with the Amplex Red data, this suggest that H₂O₂ is not involved in the DNA photocleavage reaction. Catalase in this experiment enhances cleavage, which we attribute to the presence of active copper ions in this enzyme.

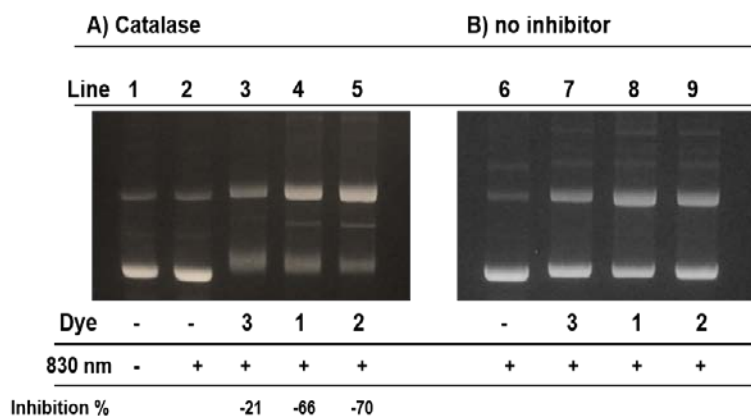


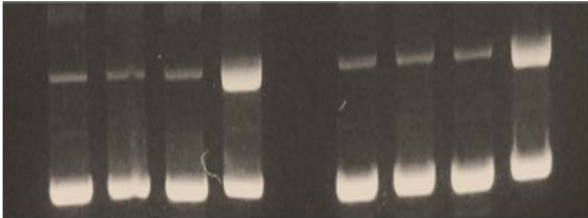
Figure 3.18 Photographs of 1.5% nondenaturing agarose gel with catalase. Each of the samples was prepared in the presence of 10 mM sodium phosphate buffer pH 7.0 and 38 μ M bp pUC19 DNA, 20 μ M of compound, in a 20 μ L reaction volume. The concentration of catalase was 25 U/ μ L. Samples were irradiated with 300 mW, 830 nm laser in a metal block to remove heat for 30 min. Temperature was measured with a thermometer and maintained at 22⁰

C.

3.2.9 Deuterium oxide, singlet oxygen potentiator

Deuterium oxide (D₂O) is usually used as a solvent for photochemical reaction experiments. The deuterium solvent effect is an important tool to investigate the mechanism of photochemical reactions. The lifetime of ¹O₂ is 10 times longer in deuterium oxide (D₂O) than in H₂O. [58] Therefore detecting singlet oxygen (¹O₂) is straight forward in D₂O. So, if in aqueous

solution, a photocleavage reaction is dependent on singlet oxygen, carrying out the procedure in D₂O should enhance the reaction considerably by increasing DNA photocleavage yields. Figures 3.19 and 3.20 show the gel pictures of the compound **1** and **2** in the presence of D₂O and H₂O. Since D₂O does not significantly enhance cleavage yield, we can conclude that singlet oxygen is not involved in dye **1** and **2** photocleavage reaction. The low levels of photocleavage inhibition generated by the singlet oxygen scavenger, sodium azide, is likely to involve side reacting with other reactive oxygen species other than singlet oxygen. (Figure 3.16)

Lane	1	2	3	4	5	6	7	8
Cleavage (%)	9	8	9	65	11	10	12	69
								
Dye	-	+	-	+	-	+	-	+
830 nm	-	-	+	+	-	-	+	+
H ₂ O	+	+	+	+	-	-	-	-
D ₂ O	-	-	-	-	+	+	+	+

*Figure 3.19 DNA photocleavage by Compound **1** in the presence and absence of D₂O 70% (v/v). Samples contained 38 μ M bp pUC19 plasmid DNA, 20 μ M dye **1**, sodium phosphate buffer pH 7.0, 100% (v/v) ddH₂O (lanes 1, 2, 3, 4) and 70% (v/v) D₂O (lanes 5, 6, 7, 8). Samples were irradiated with 300 mW, 830 nm laser in a metal block to remove heat for 30 min. Temperature was measured with a thermometer and maintained at 22⁰ C .*

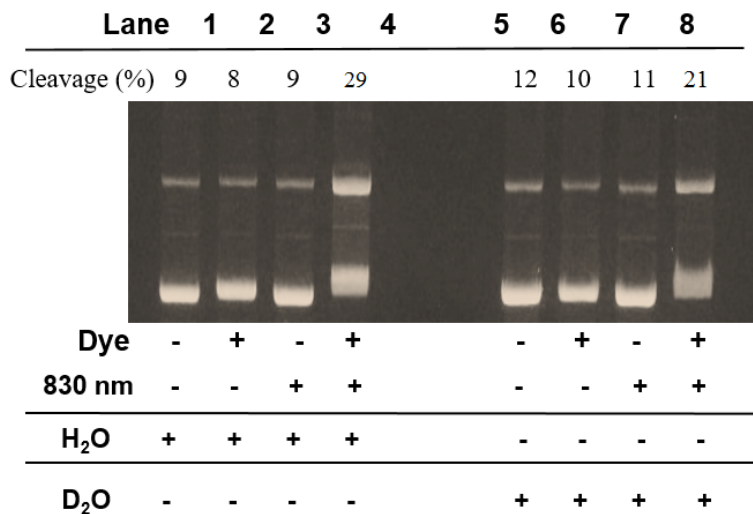


Figure 3.20 DNA photocleavage by Compound 2 in the presence and absence of D₂O 70% (v/v). Samples contained 38 μ M bp pUC19 plasmid DNA, 20 μ M dye 2, sodium phosphate buffer pH 7.0, 100% (v/v) ddH₂O (lanes 1, 2, 3, 4) and 70% (v/v) D₂O (lanes 5, 6, 7, 8). Samples were irradiated with 300 mW, 830 nm laser in a metal block to remove heat for 30 min. Temperature was measured with a thermometer and maintained at 22 °C .

3.2.10 Anaerobic photocleavage of plasmid DNA using a glove box

An anaerobic chamber or glove box was designed to run out DNA photocleavage experiments under anaerobic conditions in an argon flow and under aerobic condition in air flow. In this series of experiment, our goal was to clarify the effects of oxygen in photocleavage activities of compounds **1** and **2**. Photocleavage inhibition by the hydroxyl radical scavenger sodium benzoate was moderate (Figure 3.16); the Amplex Red and catalase experiments ruled against the participation of H₂O₂ (Figures 3.17, 3.18); and the D₂O experiment ruled out the involvement of singlet oxygen (Figure 3.19). So we ran two separate experiments in the glove box. In the first experiment, we prepared and irradiated samples in the glove box with argon flow in the chamber. All ddH₂O and buffer solutions were purged with argon using a gas bubbler. In the second series of experiments, we changed argon flow to air flow, the solutions were bubbled

with air. Then we prepared and irradiated our samples in the air flow in the chamber. Samples contained 38 μM bp pUC19 plasmid DNA, 20 μM dyes **1** and **2**, and 10 mM sodium phosphate buffer pH 7.0. Samples were irradiated with the 830 nm laser in the glove box.

As it is shown in Figure 3.21, the cleavage percentage with argon flow in the chamber is significantly lower than cleavage under the aerobic conditions. Anaerobic conditions dramatically decreased the photocleavage activity of both compounds **1** and **2**.

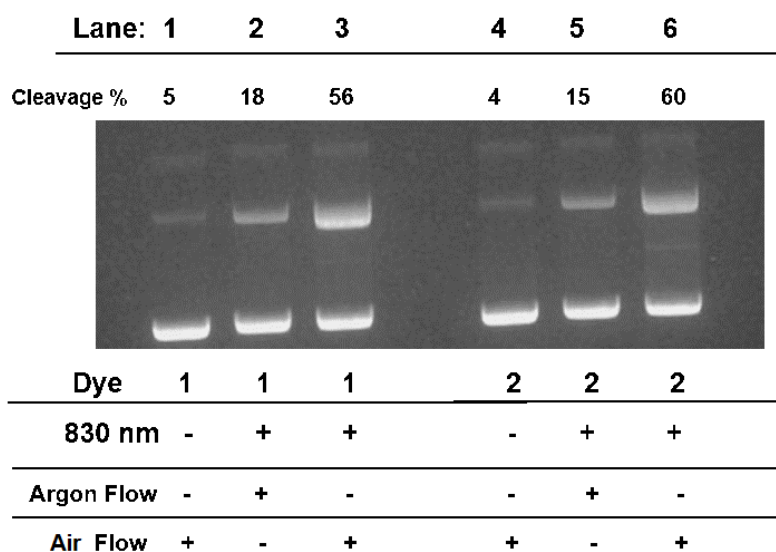


*Figure 3.21 Aerobic and anaerobic cleavage experiments using glove box. Samples contained 38 μM bp pUC19 plasmid DNA, 20 μM dye **1** and **2**, and sodium phosphate buffer pH 7.0. Samples were prepared inside the glove box and irradiated with 300 mW, 830 nm laser in a metal block to remove heat for 30 min. Temperature was measured with a thermometer inside the metal block and maintained at 22⁰ C.*

Table 2. Average inhibition % of DNA photocleavage induced by ROS scavengers, D₂O, catalase and anaerobic conditions in glove box.

Reagent	Species targeted	Average photo cleavage inhibition (%)	
		Dye 1	Dye 2
Sodium benzoate (100 mM)	$\cdot\text{OH}$	31%	40%
Sodium azide (100 mM)	$^1\text{O}_2$	26%	24%
D ₂ O (70% v/v)	$^1\text{O}_2$	-4%	10%
Catalase (2.5 u/ μL)	H ₂ O ₂	-60%	-67%
Anaerobic Photocleavage with Argon	O ₂	67%	75%

Based on the percentage cleavage inhibition in Table 2, anaerobic photocleavage has a great inhibitory effect on photocleavage, which strongly indicates the involvement of oxygen in the cleavage reactions. Singlet oxygen scavengers and H₂O₂ detectors ruled out presence of singlet oxygen and H₂O₂. The sodium benzoate data suggest that hydroxyl radical are involved.

3.2.11 CT DNA absorption titration and induced circular dichroism data

In order to determine the binding modes of our compounds, we recorded induced circular dichroism (ICD) and circular dichroism spectra (CD). The exact position and orientation of a ligand and the environment within its binding site greatly affect the ICD of a DNA bound ligand. Before running the experiment, we needed to get the saturation point when all of the dyes were 100% bound to CT-DNA. Thus, in the UV-visible DNA titration experiments, small volumes of an aqueous stock solution of CT DNA were sequentially added to samples containing 10 μM of dye **1** and **2** and 10 mM of sodium phosphate buffer pH 7.0. Final concentrations of CT DNA in each sample ranged from 0 μM bp up to 140 μM bp. On adding the solution of CT-DNA, decreases in absorption intensity of dyes **1** and **2** were observed. The total volume of the cuvette before adding DNA was 500 μL . UV-visible absorption spectra were recorded from 200 nm to

1100 nm. The result of UV-visible were collected from sample dilution arising from DNA dilution. Figure 3.22 and Appendix Figures 0.1 and 0.3 show UV-visible absorption change, stop at 120 μM bp, indicating that dyes **1** and **2** are completely bound to DNA.

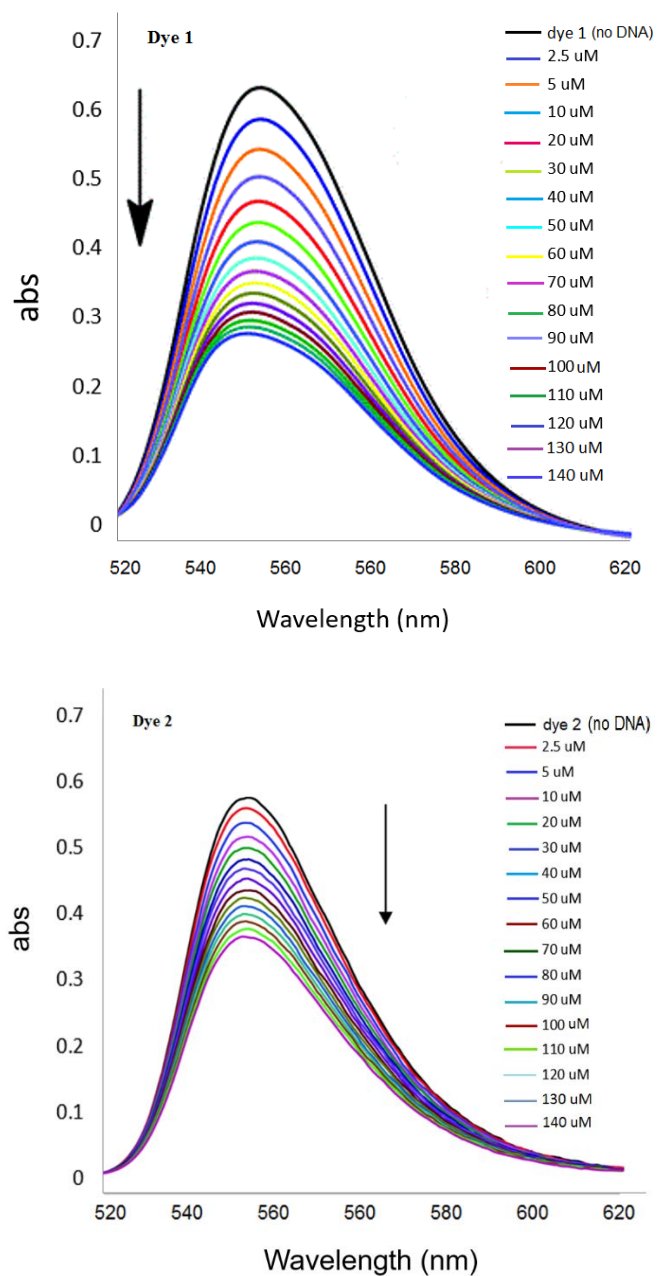


Figure 3.22. CT DNA concentration titration of dye 1 and dye 2. Individual samples contained 10 mM sodium phosphate buffer pH 7.0, 10 μM of dye 1 and 2 and increasing concentrations of CT DNA from 0 to 140 μM bp.

The absorption data in Figure 3.22 show that cyanine dyes **1** and **2** are interacting with DNA but did not provide evidence in favor of finding DNA binding mode. In order to address this, we recorded circular dichroism and induced circular dichroism spectra of 10 μM of dye **1** or **2**, equilibrated with 120 μM bp of CT DNA (Figure 3.23). The amplitude of the induced CD of dye **1** much greater than for compound **2** at the same mixing ratio and dye concentration. Pentamethine and cyanine dyes are well-known in DNA intercalators and groove binders. Minor groove binders, have limited flexibility, allowing the molecules to adjust structure to follow the groove as it twists around the central axis of the helix. When dimer or higher order complexes are formed with DNA, minor groove cyanine dyes produce a bisignate induced exciton CD signal. An exciton CD is indicative of the formation of dimer, or higher order complexes. [48] The ICD spectra of compounds **1** and **2** generate induced bisignate curves (change of sign within the band) with one positive and one negative band located on either side of the absorption maximum of the free ligand. (Figure 3.23) Garbet et al. pointed out that this is the result of the proximity of two identical transition moments of equal energy. [48]

These induced CD measurements indicated the binding mode of complexes with CT-DNA might involve the DNA minor groove. [48], [60] The induced CD data taken together with the UV-visible absorption and photocleavage results indicate that there are two DNA binding modes for **1** and **2**. Intercalation is typically, observed for cationic molecules that have planar aromatic rings. Intercalators will often exhibit lower intensity CD spectra compare with groove binders and this is most likely due to the fact that a groove binder contacted a larger part of the helix. [1], [61] The CD signal at 280 nm is the DNA signal and the reduction in the DNA CD signal suggests that some of the cyanine dye molecules are binding to DNA by intercalation. Binding the minor groove requires substantially less distortion of the DNA compared with

intercalative binding. [62], [61], [1] Most intercalators reduce the helical twist angle of the DNA, resulting in a reduction in the intensity of the DNA signal at 280 nm. [63], [64] On the other hand, groove binding have strong CD signal because they cover more space in the groove. The bisignate induced ICD at 550 nm points to groove binding of a dimer or higher order cyanine dye aggregate to the DNA minor groove. The reduction in the CD signal at 280 nm points to intercalation.

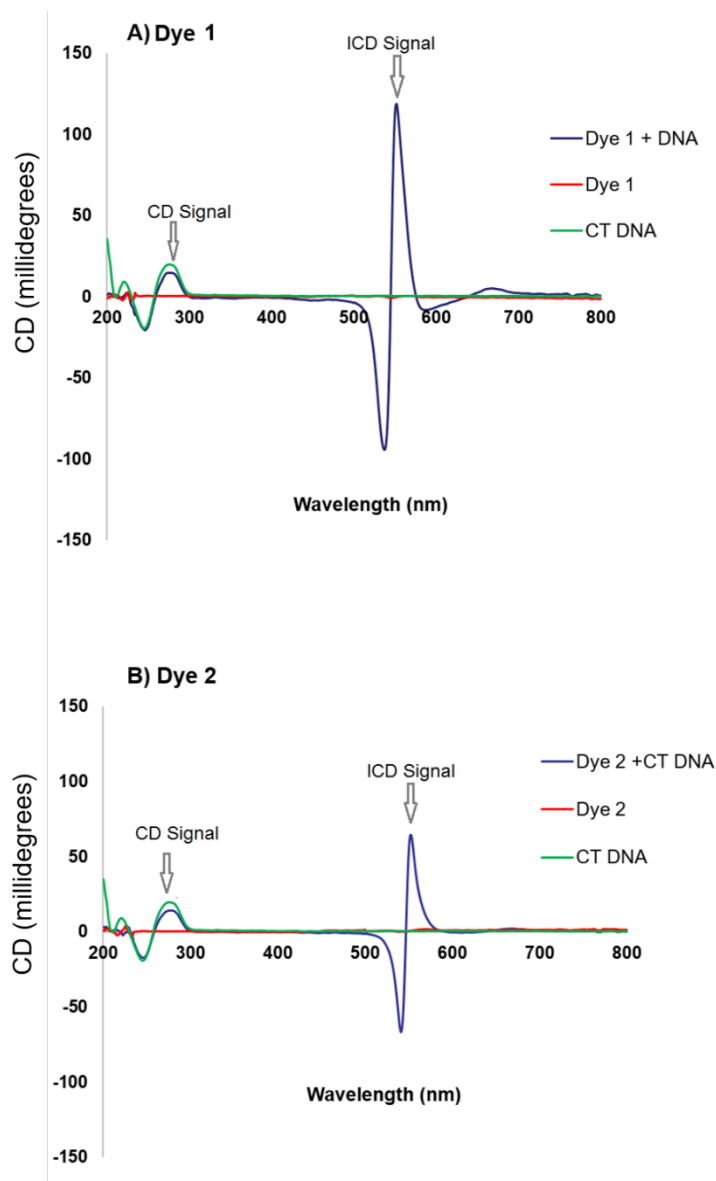


Figure 3.23. Circular dichroism (CD) spectra of A) dye **1** and B) dye **2** in the presence and absence of DNA.

Spectra recorded at 22 °C of 10 μM of **1** and **2** in the presence and absence of 120 μM of CT-DNA and 10 mM sodium phosphate buffer pH.7.0.

3.2.12 Determination of the dye binding constants (K_b)

Binding constant (K_b) is a measure of the dye–DNA complex stability. In order to estimate the binding constants of dyes **1** and **2**, the titration data were fit to absorption model of Meehan and coworkers. [50] The experimental determination of the binding constant of a cyanine dye for its target is considerable importance. The association of **1** and **2** with DNA was

studied by CT-DNA titrations using UV-Vis spectrometry. In these experiments, increasing concentration of DNA were added to fixed concentration of cyanine dye. Binding constants (K_b) were calculated from changes in absorbance of cyanine dyes. Figures 3.24 and 3.25 show the binding constant over three trials of Cl and Br compounds **1** and **2**. The original UV-visible titrations are in Appendix (Figure 0.1). The calculated binding constants suggest that compound **1** has more affinity for DNA than compound **2**. Compound **1** also generate a much stronger ICD signal than **2** (Figure 3.23).

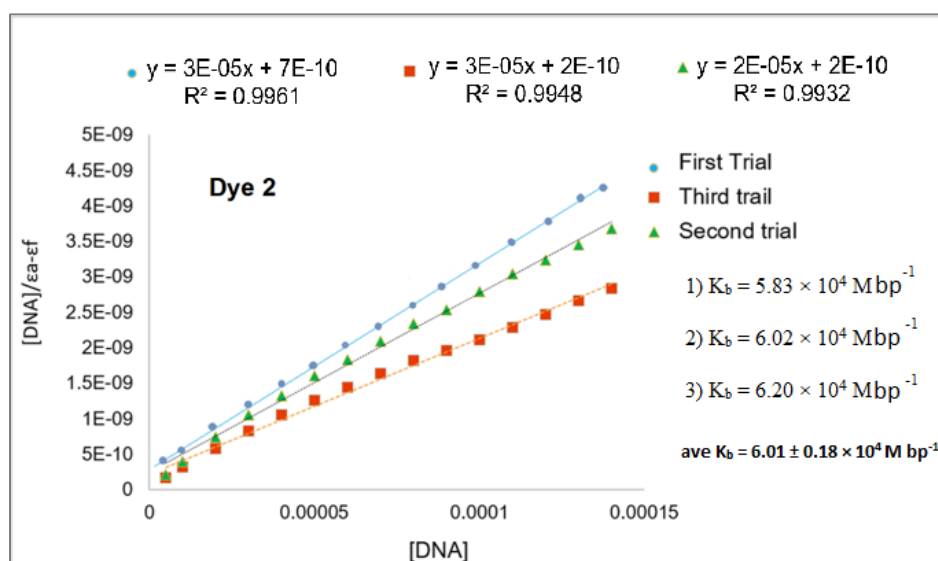
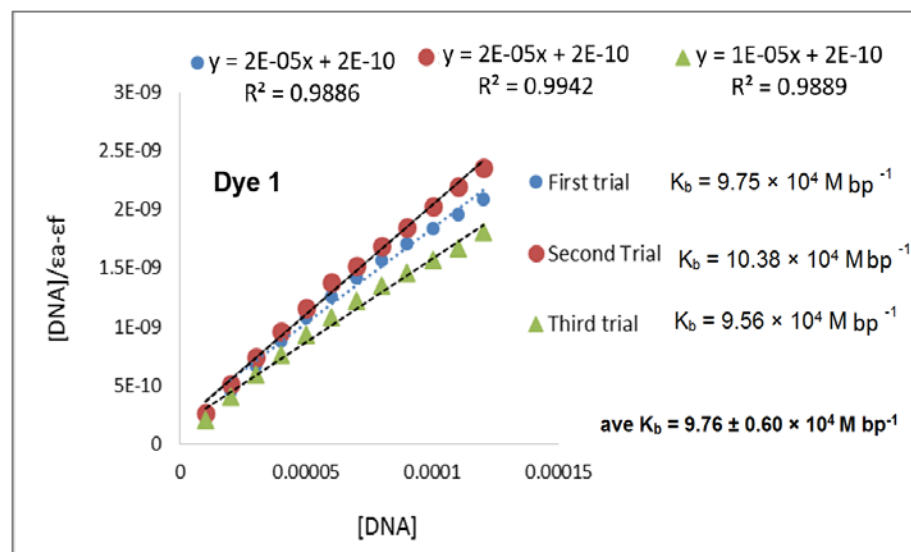


Figure 3.24 Representative plots for the interaction of 120 μM of CT-DNA and 10 μM of dye **1** and **2** and 10 mM of sodium phosphate buffer, pH 7.0. Linear fitting to Meehan and coworker's binding model generated the curves shown above. The plots were prepared using absorbance at the λ_{max} value of the dyes **1** and **2**.

4 CONCLUSIONS

The purpose of our research was to evaluate the interactions between quinoline cyanine dyes and DNA. We focused on cyanine dyes absorbing infrared light to get deep penetration through biological tissue. These dyes are potentially important as therapeutic agents in photodynamic therapy. We identified series of cyanine dyes containing quinoline that bound to DNA. When a hydrogen atom was present at the meso position of the dye's polymethine bridge, the cyanine was easily oxidized and decomposed even when DNA was present. The halogen substituted dyes were shown to bind to the DNA most likely within the minor groove by forming dimers or more complex aggregates. DNA intercalation by the dyes was also indicated. Time course UV-visible absorbance spectra of H, Cl and Br cyanine dyes showed that our cyanine dyes are not very stable in aqueous buffer systems. However when we added CT-DNA to the aqueous buffer, the halogen substituted dyes were stable. Agarose gel electrophoresis showed that we achieved high levels of photocleavage of DNA with the halogenated dyes at wavelengths as long as 830 and 850 nm. These are the longest wavelengths ever to be used to photo-cleave DNA. [17] The reaction were completed after 5 min of irradiation. The photo cleavage was time-dependent. Temperature dependent experiments showed that our dyes are photo chemically active even at 10 °C. Scavenger studies pointed to the participation of reactive oxygen species, particularly hydroxyl radicals in the photocleavage reactions. Hydrogen peroxide and singlet oxygen participation could not be confirmed. Anaerobic experiment strongly pointed to O₂ involvement. Based on the data acquired, some trends were indicated with respect to the structure activity correlations. Specifically, we found that introducing a halogen substituent at the meso position of the polymethine bridge of quinoline cyanine dyes, dramatically increased the photo cleavage activity most likely by stabilizing the dyes. The yield of DNA photocleavage by

dye **1** and **2** are close to each other. We also found our compounds bound to DNA and producing strong CD and ICD signal suggesting groove binding and intercalation. In conclusion, developing efficient NIR photosensitizing agents for PDT is highly demanded. It allows for excitation dyes with NIR light, which greatly increases tissue penetration depth in PDT. Our results are important since they provide a simple strategy for using the resource of NIR irradiation in photodynamic cancer therapy.

REFERENCES

1. Armitage, B.A., Cyanine dye–DNA interactions: intercalation, groove binding, and aggregation, in DNA binders and related subjects. 2005, Springer. p. 55-76.
2. Herz, A., Dye-dye interactions of cyanines in solution and at AgBr surfaces. *Photographic Science and Engineering*, 1974. 18(3): p. 323-335.
3. Kawabe, Y. and S. Kato, Spectroscopic study of cyanine dyes interacting with the biopolymer, DNA. *Dyes and Pigments*, 2012. 95(3): p. 614-618.
4. Behera, G., P. Behera, and B.K. Mishra, Cyanine Dyes: Self Aggregation and Behaviour in Surfactants A Review. *Journal of Surface Science and Technology*, 2007. 23(1/2): p. 1.
5. Liu, J.-G., et al., Enantiomeric ruthenium (II) complexes binding to DNA: binding modes and enantioselectivity. *JBIC Journal of Biological Inorganic Chemistry*, 2000. 5(1): p. 119-128.
6. Kaloyanova, S., et al., Synthesis and study of nucleic acids interactions of novel monomethine cyanine dyes. *Dyes and Pigments*, 2012. 92(3): p. 1184-1191.
7. Mapp, C.T., et al., Oxidative cleavage of DNA by pentamethine carbocyanine dyes irradiated with long-wavelength visible light. *Bioorganic & Medicinal Chemistry Letters*, 2014. 24(1): p. 214-219.
8. Williams, C.G., XXVI.—Researches on Chinoline and its Homologues. *Transactions of the Royal Society of Edinburgh*, 1857. 21(03): p. 377-401.
9. Kim, M., H.Y. Jung, and H.J. Park, Topical PDT in the Treatment of Benign Skin Diseases: Principles and New Applications. *International Journal Of Molecular Sciences*, 2015. 16(10): p. 23259-23278.

10. Jang, W.-D., et al., Polyion complex micelles for photodynamic therapy: incorporation of dendritic photosensitizer excitable at long wavelength relevant to improved tissue-penetrating property. *Journal of Controlled Release*, 2006. 113(1): p. 73-79.
11. Schmidt-Erfurth, U. and T. Hasan, Mechanisms of action of photodynamic therapy with verteporfin for the treatment of age-related macular degeneration. *Survey of Ophthalmology*, 2000. 45(3): p. 195-214.
12. Svaasand, L.O., C.J. Gomer, and E. Morinelli, On the physical rationale of photodynamic therapy. *Future Directions and Application in Photodynamic Therapy*. CJ Gomer (Ed.). SPIE Institute Series for Advanced Optical Technologies, IS6, 1990: p. 233-248.
13. Henderson, B.W. and T.J. Dougherty, How does photodynamic therapy work? *Photochemistry and Photobiology*, 1992. 55(1): p. 145-157.
14. Castano, A.P., T.N. Demidova, and M.R. Hamblin, Mechanisms in photodynamic therapy: part one—photosensitizers, photochemistry and cellular localization. *Photodiagnosis and Photodynamic Therapy*, 2004. 1(4): p. 279-293.
15. Yoon, I., J.Z. Li, and Y.K. Shim, Advance in photosensitizers and light delivery for photodynamic therapy. *Clinical Endoscopy*, 2013. 46(1): p. 7-23.
16. König, K., *Handbook of Biomedical Nonlinear Optical Microscopy*. 2008, New York: Oxford University Press.
17. Li, Z. and K.B. Grant, DNA photo-cleaving agents in the far-red to near-infrared range—a review. *RSC Advances*, 2016. 6(29): p. 24617-24634.
18. Schaffer, M., et al., Application of Photofrin II as a specific radiosensitising agent in patients with bladder cancer—a report of two cases. *Photochemical & Photobiological Sciences*, 2002. 1(9): p. 686-689.

19. Hofstetter, A., et al., Use of photofrin as a radiosensitizer. 2001, Google Patents.
20. Bressler, N.M., S.B. Bressler, and S.L. Fine, Age-related macular degeneration. *Survey of Ophthalmology*, 1988. 32(6): p. 375-413.
21. Hopper, C., Photodynamic therapy: a clinical reality in the treatment of cancer. *The Lancet Oncology*, 2000. 1(4): p. 212-219.
22. Tan, I.B., et al., Temoporfin-mediated photodynamic therapy in patients with advanced, incurable head and neck cancer: A multicenter study. *Head & neck*, 2010. 32(12): p. 1597-1604.
23. Wang, S., et al., Talaporfin sodium. *Expert opinion on pharmacotherapy*, 2010. 11(1): p. 133-140.
24. Ulatowska-Jarza, A., et al., Spectroscopic properties of a chlorophyll-based photosensitive dye entrapped in sol-gel fibre-optic applicators. *Materials Science-Poland*, 2005. 23(1): p. 111-122.
25. Copley, L., et al., Photolon™, a chlorin e6 derivative, triggers ROS production and light-dependent cell death via necrosis. *The International Journal of Biochemistry & Cell Biology*, 2008. 40(2): p. 227-235.
26. Boni, L., et al., Clinical applications of indocyanine green (ICG) enhanced fluorescence in laparoscopic surgery. *Surgical Endoscopy*, 2015. 29(7): p. 2046-2055.
27. Alander, J.T., et al., A review of indocyanine green fluorescent imaging in surgery. *Journal of Biomedical Imaging*, 2012. 2012: p. 7.
28. Engel, E., et al., Light-induced decomposition of indocyanine green. *Investigative Ophthalmology & Visual Science*, 2008. 49(5): p. 1777-1783.

29. Agostinis, P., et al., Photodynamic therapy of cancer: an update. *CA: A Cancer Journal for Clinicians*, 2011. 61(4): p. 250-281.
30. Tegos, G., et al., Concepts and principles of photodynamic therapy as an alternative antifungal discovery platform. *Frontiers in Microbiology*, 2012. 3.
31. Fickweiler, S., et al., Photosensitization of human skin cell lines by ATMPn (9-acetoxy-2, 7, 12, 17-tetrakis-(β -methoxyethyl)-porphycene) in vitro: mechanism of action. *Journal of Photochemistry and Photobiology B: Biology*, 1999. 48(1): p. 27-35.
32. Bakalova, R., et al., Quantum dots as photosensitizers? *Nat Biotech*, 2004. 22(11): p. 1360-1361.
33. Kuo, W.S., et al., Gold nanorods in photodynamic therapy, as hyperthermia agents, and in near-infrared optical imaging. *Angewandte Chemie*, 2010. 122(15): p. 2771-2775.
34. Jin, S., et al., A new near infrared photosensitizing nanoplatform containing blue-emitting up-conversion nanoparticles and hypocrellin A for photodynamic therapy of cancer cells. *Nanoscale*, 2013. 5(23): p. 11910-11918.
35. Wang, C., et al., Near-infrared light induced in vivo photodynamic therapy of cancer based on upconversion nanoparticles. *Biomaterials*, 2011. 32(26): p. 6145-6154.
36. Tian, G., et al., Red-Emitting Upconverting Nanoparticles for Photodynamic Therapy in Cancer Cells Under Near-Infrared Excitation. *Small*, 2013. 9(11): p. 1929-1938.
37. Du, Y., et al., Near-infrared photoluminescent Ag₂S quantum dots from a single source precursor. *Journal of the American Chemical Society*, 2010. 132(5): p. 1470-1471.
38. Lovell, J.F., et al., Activatable photosensitizers for imaging and therapy. *Chemical Reviews*, 2010. 110(5): p. 2839-2857.

39. Lu, T., et al., Synthesis and photophysics of benzotexaphyrin: a near-infrared emitter and photosensitizer. *Journal of the American Chemical Society*, 2008. 130(47): p. 15782-15783.
40. Kostenich, G., et al., In vivo photodynamic therapy with the new near-IR absorbing water soluble photosensitizer lutetium texaphyrin and a high intensity pulsed light delivery system. *Journal of Photochemistry and Photobiology B: Biology*, 1997. 39(1): p. 36-42.
41. Mody, T.D. and J.L. Sessler, Texaphyrins: a new approach to drug development. *Journal of Porphyrins and Phthalocyanines*, 2001. 5(02): p. 134-142.
42. Atsumi, T., K. Tonosaki, and S. Fujisawa, Comparative cytotoxicity and ROS generation by curcumin and tetrahydrocurcumin following visible-light irradiation or treatment with horseradish peroxidase. *Anticancer Research*, 2007. 27(1A): p. 363-371.
43. Hanahan, D. and R.A. Weinberg, The hallmarks of cancer. *cell*, 2000. 100(1): p. 57-70.
44. Mohanty, J., et al., A highly sensitive fluorescent micro-assay of H₂O₂ release from activated human leukocytes using a dihydroxyphenoxazine derivative. *Journal of Immunological Methods*, 1997. 202(2): p. 133-141.
45. Zhou, M., et al., A stable nonfluorescent derivative of resorufin for the fluorometric determination of trace hydrogen peroxide: applications in detecting the activity of phagocyte NADPH oxidase and other oxidases. *Analytical Biochemistry*, 1997. 253(2): p. 162-168.
46. Mason, S., Induced circular dichroism. *Chemical Physics Letters*, 1975. 32(2): p. 201-203.

47. Johnson Jr, W.C., Secondary structure of proteins through circular dichroism spectroscopy. *Annual Review of Biophysics and Biophysical Chemistry*, 1988. 17(1): p. 145-166.
48. Garbett, N.C., P.A. Ragazzon, and J.B. Chaires, Circular dichroism to determine binding mode and affinity of ligand–DNA interactions. *Nature Protocols*, 2007. 2(12): p. 3166-3172.
49. Tedesco, D. and C. Bertucci, Induced circular dichroism as a tool to investigate the binding of drugs to carrier proteins: Classic approaches and new trends. *Journal of Pharmaceutical and Biomedical Analysis*, 2015. 113: p. 34-42.
50. Ganeshpandian, M., et al., New ruthenium (II) arene complexes of anthracenyl-appended diazacycloalkanes: effect of ligand intercalation and hydrophobicity on DNA and protein binding and cleavage and cytotoxicity. *Dalton Transactions*, 2014. 43(3): p. 1203-1219.
51. Aranki, A. and R. Freter, Use of anaerobic glove boxes for the cultivation of strictly anaerobic bacteria. *The American Journal of Clinical Nutrition*, 1972. 25(12): p. 1329-1334.
52. Wilkinson, F., W.P. Helman, and A.B. Ross, Rate constants for the decay and reactions of the lowest electronically excited singlet state of molecular oxygen in solution. An expanded and revised compilation. *Journal of Physical and Chemical Reference Data*, 1995. 24(2): p. 663-677.
53. Gorman, A., et al., In vitro demonstration of the heavy-atom effect for photodynamic therapy. *Journal of the American Chemical Society*, 2004. 126(34): p. 10619-10631.
54. Verhoeven, J., Glossary of terms used in photochemistry (IUPAC Recommendations 1996). *Pure and Applied Chemistry*, 1996. 68(12): p. 2223-2286.

55. Castano, A.P., T.N. Demidova, and M.R. Hamblin, Mechanisms in photodynamic therapy: part three—photosensitizer pharmacokinetics, biodistribution, tumor localization and modes of tumor destruction. *Photodiagnosis and Photodynamic Therapy*, 2005. 2(2): p. 91-106.
56. Bilski, P., et al., The photooxidation of diethylhydroxylamine by rose bengal in micellar and nonmicellar aqueous solutions. *Photochemistry and Photobiology*, 1993. 58(1): p. 11-18.
57. Ma, J. and L. Jiang, Photogeneration of singlet oxygen (1O_2) and free radicals ($Sen^{\cdot-}$, $O^{\cdot-2}$) by tetra-brominated hypocrellin B derivative. *Free Radical Research*, 2001. 35(6): p. 767-777.
58. Moan, J. and K. BERG, The photodegradation of porphyrins in cells can be used to estimate the lifetime of singlet oxygen. *Photochemistry and Photobiology*, 1991. 53(4): p. 549-553.
59. Rhee, S.G., et al., Methods for detection and measurement of hydrogen peroxide inside and outside of cells. *Molecules and Cells*, 2010. 29(6): p. 539-549.
60. Sovenyhazy, K.M., J.A. Bordelon, and J.T. Petty, Spectroscopic studies of the multiple binding modes of a trimethine-bridged cyanine dye with DNA. *Nucleic Acids Research*, 2003. 31(10): p. 2561-2569.
61. Geierstanger, B.H. and D.E. Wemmer, Complexes of the minor groove of DNA. *Annual Review of Biophysics and Biomolecular Structure*, 1995. 24(1): p. 463-493.
62. Lerman, L., Structural considerations in the interaction of DNA and acridines. *Journal of Molecular Biology*, 1961. 3(1): p. 18IN13-30IN14.

63. Terry, C.A., et al., Physiologically relevant concentrations of NaCl and KCl increase DNA photocleavage by an N-substituted 9-aminomethylantracene DYE. *Biochemistry*, 2011. 50(47): p. 10375-10389.
64. Johnson, B.B., et al., Correlations between deoxyribonucleic acid structural parameters and calculated circular dichroism spectra. *Biochemistry*, 1981. 20(1): p. 73-78.

APPENDICES

Appendix A

Appendix A.1

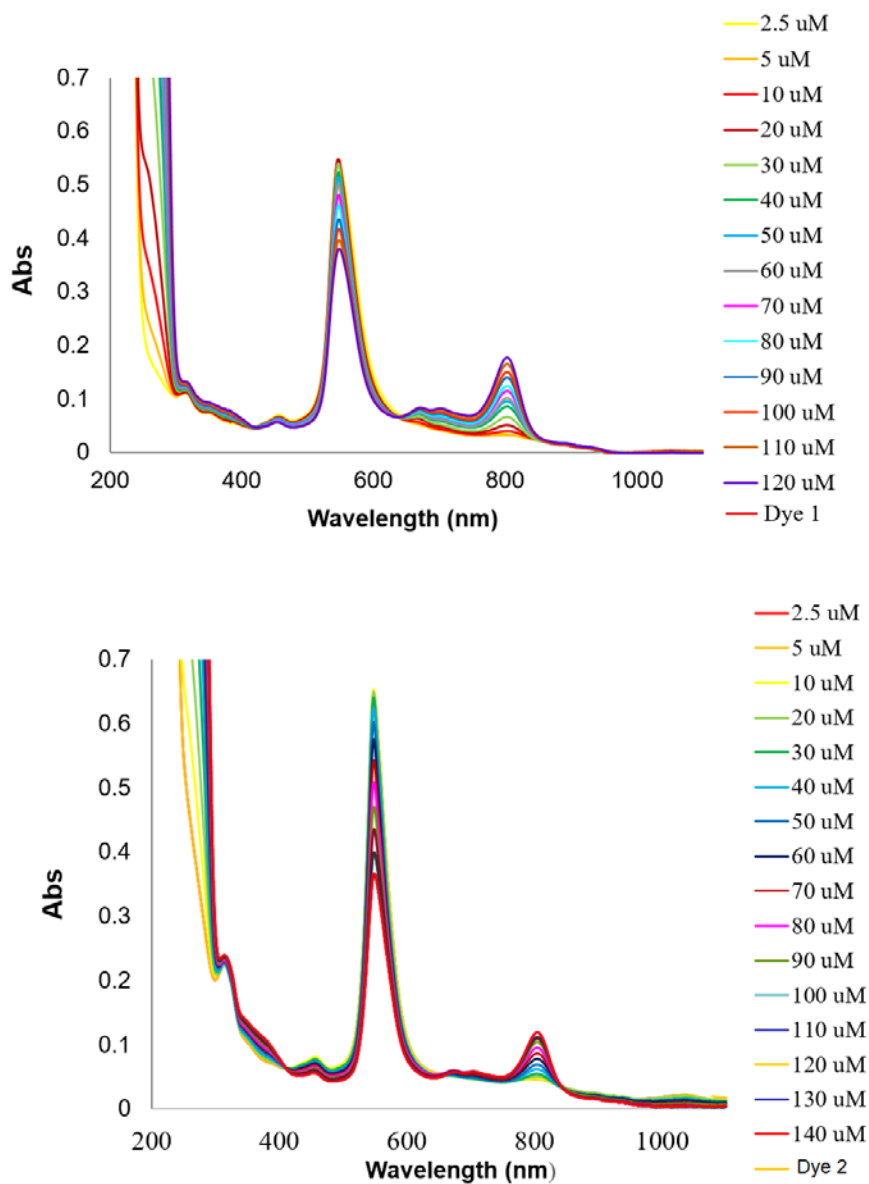


Figure 0.1 CT-DNA concentration titration of dyes 1 and 2 from 200 nm to 1100 nm
Individual samples contained 10 mM sodium phosphate buffer pH 7.0, 10 μM of dye 1
and 2 and increasing concentration of CT-DNA from 0 to 120 μM bp.

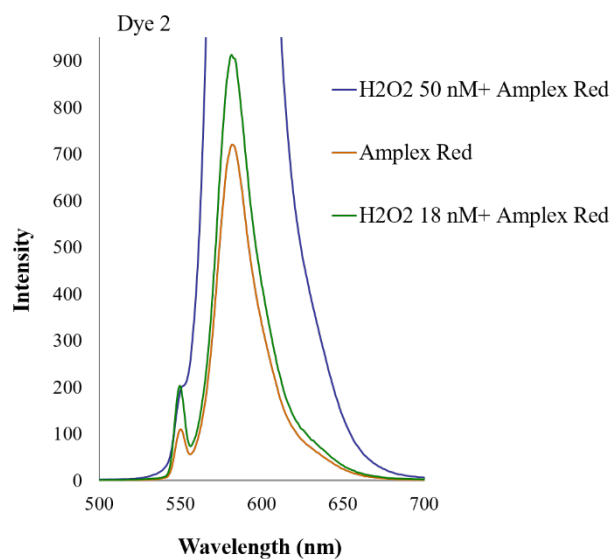
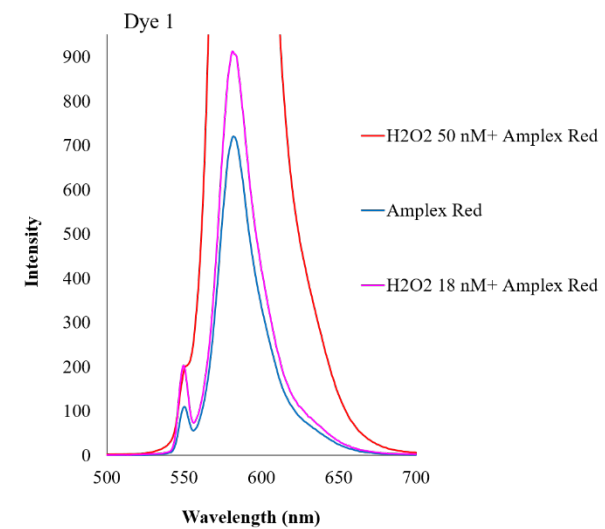


Figure 0.2 control experiment for H_2O_2 detection using Amplex Red.

260 μ L of Amplex Red cocktail containing 100 μ M Amplex Red and 2 U/mL horseradish peroxidase (HRP) in 50 mM sodium phosphate buffer pH 7.0 was prepared. 50 nM and 18 nM of H_2O_2 were added to the reaction right before running the instrument. 350 μ L of each reaction was then diluted in a cuvette with 50 mM sodium phosphate buffer to a total volume of 3000 μ L.

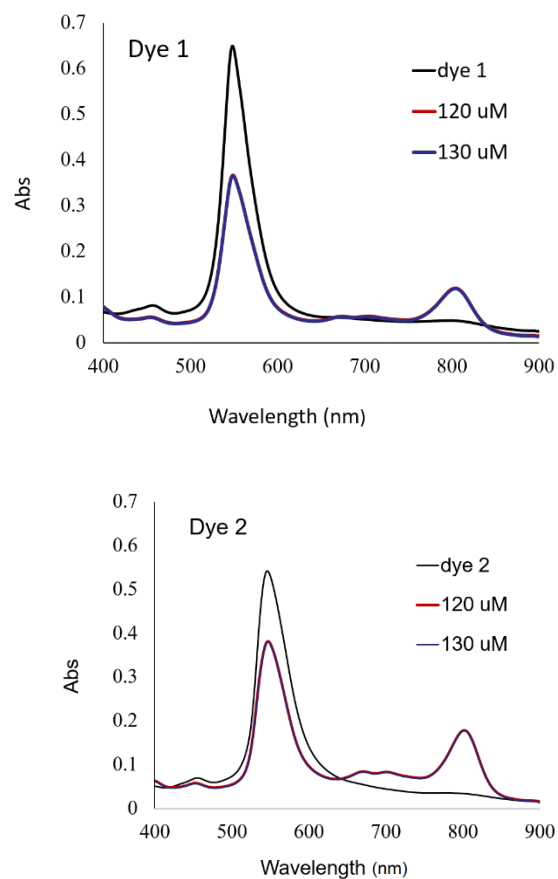


Figure 0.3 CT-DNA concentration titration of dye 1 and 2 from 400 nm to 900 nm. Individual samples contained 10 mM sodium phosphate buffer pH 7.0, 10 μ M of dye 1 and 2 and increasing concentration of CT-DNA from 0 to 120 μ M bp.